NASA CR-66040

RESULTS OF HEAT TRANSFER TESTS ON SHARP AND SPHERICALLY BLUNTED 4° HALF ANGLE CONICAL MODELS IN A PLASMA JET AND IN A HYPERVELOCITY WIND TUNNEL

LTV REPORT NO. 00.725
17 December 1965

Prepared by:

J. C. Hester

D. M. Martin

Reviewed by:

J. K. Haviland

Approved by:

K. M. Russ

Prepared by LTV Astronautics Division under Contract Number NAS1-3915, Work Item 9, Graphite Nose Tip Heating and Aerodynamic Tests

TABLE OF CONTENTS

LIST OF FIGURES

LIST OF FIGURES (Continued)

LIST OF TABLES

RESULTS OF HEAT TRANSFER TESTS ON SHARP AND SPHERICALLY BLUNTED 4° HALF ANGLE CONICAL MODELS IN A PLASMA JET AND IN A HYPERVELOCITY WIND TUNNEL

By J. C. Hester and D. M. Martin
LTV Astronautics Division
LTV Aerospace Corporation

SUMMARY

16586

A series of heating tests was conducted on slender conical models to provide technical data for evaluation of the performance of relatively sharp nose tips during entry at hypersonic speeds. The work was performed under Contract NAS1-3915 with NASA Langley Research Center.

High Mach number (14 to 17) tests were conducted in a hypervelocity wind tunnel at Reynold's numbers per foot of 0.1×10^6, 1×10^6 and 3×10^6. High heating rate tests were conducted on ATJ graphite models in the LTV plasma facility at a Mach number of 3.0.

The data were shown to compare well with existing theories if the effects of viscous interaction and slip flow were considered. The data were also compared to the previous results of Medford and Holt, who deduced heating rates from mass loss data, and the results were found to be compatible.

Based upon the results of these tests, a theory was postulated which predicts that a pointed tip will remain pointed so long as the distance from the tip to the point where continuum effects begin is much greater than the nose radius.

Predictions of the performance of an 0.001 inch nose radius graphite tip were made which indicated that a sharp configuration would exist down to an altitude of approximately 40,000 feet, at which time blunting would begin.

This contract was administered by the Langley Research Center under the technical direction of Mr. C. B. Rumsey of the Applied Materials and Physics Division.

Author

1.0 INTRODUCTION

The study reported here was conducted for the NASA Langley Research Center under the Dallas Support portion of Contract NAS1-3915 to provide technical data for evaluation of the performance of sharp nose tips currently under investigation in conjunction with a re-entry flight experiment at a velocity of approximately 20,000 fps.

One requirement to attain the flight experiment objectives is that the high entropy layer about the body be thin. Since this entropy layer thickness is proportional to the nose radius, it is essential that the nose tip maintain a relatively pointed configuration during re-entry. One of the materials being considered for the nose tip of the re-entry vehicle is graphite.

Previous studies (Reference 1) presented mass loss rates and shape charges for graphite tips which were obtained at a low Mach number. Since oxidation theory predicts that the mass loss and accompanying shape changes of the graphite tip be proportional to the heating rates, the present study was conducted to obtain heat transfer data for Mach numbers comparable to those expected during atmospheric re-entry. This study was also conducted to verify the results of Reference 1 as well as to suggest modifications to existing heat transfer theories as applied to slender noses. The results may then be used to predict the performance of graphite nose tips during atmospheric re-entry.

Heating distributions were obtained at high Mach numbers in the hypervelocity wind tunnel and at high heating rates in the LTV plasma facility. Modifications resulting from rarefied flow and viscous interaction effects were applied to the theories of Fay and Riddell, Lees, and Van Driest and the results were shown to agree with the data.

The sharp pointed graphite model remained sharp in the plasma tests, and a theory was postulated to explain this phenomenon. This theory, which is based on a slip flow analysis near the stagnation point, was then applied to predict the performance of a sharp pointed graphite model during re-entry. The hypothesis advanced here leads to the conclusion that a graphite tip with a nose radius of 0.001 inches will, providing the tip material has sufficient strength to withstand the aerodynamic loading, remain sharp down to an altitude of approximately 40,000 feet at which time blunting will begin.

LIST OF SYMBOLS

h	=	enthalpy BTU/lb
k	=	thermal conductivity of the gas BTU/ft-sec - °F
M	=	Mach Number
$\dot{q}$	=	heat transfer rate BTU/ft^2 - sec
R	=	nose radius
R_e	=	Reynolds Number
$\widetilde{N}_u$	=	effective Nusselt Number (Eq. 5)
$\widetilde{N}_R$	=	effective Reynolds Number (Eq. 6)
S_t	=	Stanton Number = $\dot{q}/\rho U \Delta h_g$
S'	=	distance from virtual tip
P	=	total pressure - psf
p	=	static pressure - psf
x	=	distance - ft
θ	=	angle radians
C_p	=	specific heat
λ	=	mean free path
ρ	=	density-slugs/ft^3
μ	=	viscosity
γ	=	ratio of specific heats
U	=	velocity ft/sec
g	=	gravitational constant
J	=	conversion factor

C = Chapman - Rubesin viscosity coefficient

d_c = $\cdot \frac{968}{M_c^2} \frac{T_w}{T_c} + .145\,(\gamma-1)$, parameter in boundary-layer displacement analysis, Ref. 7

$F_1(K)$ = parameter in boundary-layer displacement analysis, Ref. 7

$\bar{\chi}$ = $M^3 \Big/ \sqrt{C/R_e}$, hypersonic interaction parameter

LIST OF SUBSCRIPTS

s = stagnation value

w = value at wall

ℓ = local value

∞ = free stream value

c = cone value

v = viscous interaction value

2.0 TEST APPARATUS, MODELS AND TECHNIQUES

Heat transfer tests were conducted in both the hypervelocity wind tunnel* and the LTV plasma facility. The tests were designed to evaluate the effects of Mach number and Reynolds number on the performance of various nose tips.

2.1 PLASMA ARC TESTS

Tests were conducted on "ATJ" grade graphite models in the LTV Plasma Facility using a 77% nitrogen and 23% oxygen gas having a stagnation enthalpy of approximately 12,000 BTU/lb at a Mach number of 3.0. A complete discussion of this facility is presented in Reference 2. Two models with nose radii of .065 and .10 inches were tested, as were two sharp-nosed models with nose radius of approximately .001 inches. Heat transfer values were obtained using copper calorimeters as shown in Figure 1. The calorimeters were located at the stagnation point of the 0.065 and 0.10 inch nose radius models and at a distances of 1.5 and 3.5 inches from the virtual tip on all the models. The calorimeters were approximately 0.05 inch diameter copper slugs to which were attached chromel-alumel thermocouples. The calorimeters were flush fitted into the graphite model and attached with insulating cement (Sauereisen) to reduce conduction through the sides. The aft side calorimeter was rotated 90° with respect to the forward one to minimize interference effects.

The plasma tests were conducted in the following manner. Calibration runs were made in which measurements of the heat transfer rate to a 3/4 inch diameter flat-face calorimeter were related to a stagnation pressure which was measured in the plasma stream. Since only two retractable stings were available for the test, the stagnation pressure probe was removed, and a test model was inserted in its place.

After the plasma jet again reached steady operation, the flat-face calorimeter was inserted into the stream and a value of the heat transfer rate to the calorimeter ($\dot{q}_{cal}$) was obtained. From this reading both the stagnation enthalpy and stagnation pressure were obtained. The graphite model was then inserted into the plasma stream for approximately fifty seconds. All the heating rate data was obtained during the first three seconds of the test. After approximately three seconds the stagnation point calorimeters melted and at approximately twenty seconds melting occurred at the side calorimeter positions. Due to the effects of erosion around the cavities produced by the calorimeters, the mass loss rates presented in the Data Section for the blunted models indicate relative effects only.

Two sharp-nosed graphite models were exposed to the plasma stream for 38 seconds to condition the surface of these models for subsequent tests in the HVWT to evaluate the effects of surface condition on the flow field. Prior to these tests, Schlieren studies were made of the flow around the unconditioned models in the HVWT. These tests are described in more detail in the HVWT test program below.

* Abbreviated to HVWT in this report

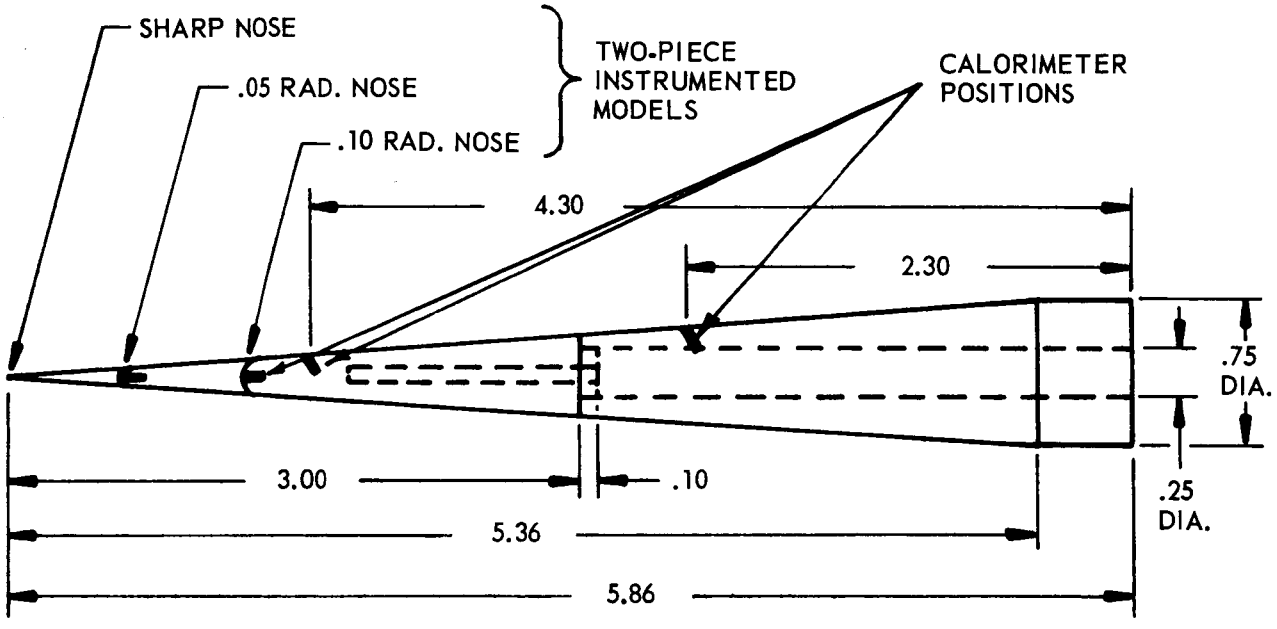

FIGURE 1 PLASMA GRAPHITE MODEL DESIGN DETAILS

2.2 HYPERVELOCITY WIND TUNNEL (HVWT) TESTS

The effects of high Mach number on the entry performance of slender cones were investigated. Heat transfer data were obtained for three instrumented specimens having nose radii of .15, .10, .05 inches and for a sharp-nosed specimen. The details of the heat transfer model are shown in Figure 2. The model consisted of a common base section with interchangeable nose sections (noses A, B, C, and D). Nose A had a solid copper calorimeter at the tip 0.358 inches in length. The base of the tip calorimeter was drilled to a depth of approximately 0.10 inches and a thermocouple imbedded in the hole such that the bead was approximately 0.25 inches aft of the forward tip. Nose B (0.05 inch radius) had a 0.026 inch diameter copper slug calorimeter at the stagnation point while Noses C and D (0.10 and 0.15 inch radii, respectively) had stagnation point and tangent point calorimeters. The stagnation point calorimeters were 0.035 and 0.051 inches in diameter respectively, while the tangent point calorimeters had a diameter of 0.024 inches. The slug calorimeters were thermally isolated from the remainder of the copper nose sections by means of boron nitride sleeves as shown in Figure 2.

The common base section was constructed of nylon which was then covered with a thin (0.0045 inch typical) copper skin. Constantan wires were attached to the underside of the copper skin at the stations indicated in Figure 2 and fed out through a cutout in the nylon as shown in Section A-A of Figure 2. By this technique, the skin of the model is included in the thermo-electric circuit so that only one thermocouple wire is required for each heat sensing station.

A photograph showing the sizes of the nose sections is presented as Figure 3. Figure 4 shows the complete heat transfer model with the various interchangeable nose sections and associated hardware.

Schlieren photographs were made of the flow field around a sharp-nosed graphite model both before and after the model has been exposed to the total heat load anticipated for a typical entry trajectory down to an altitude of approximately 60,000 feet. These results are also presented in Section 3.0.

A complete description of the test facility and of its operating characteristics is presented in Reference 3.

Heating rate data were obtained at the stagnation point and at various points along the conical section (see Figure 2 for locations) of each model at three different Reynolds numbers for each test model. Test conditions and heat transfer data resulting from these tests are presented in Section 3.0. Shown in Figure 5 is a photograph of a typical model installed in the HVWT.

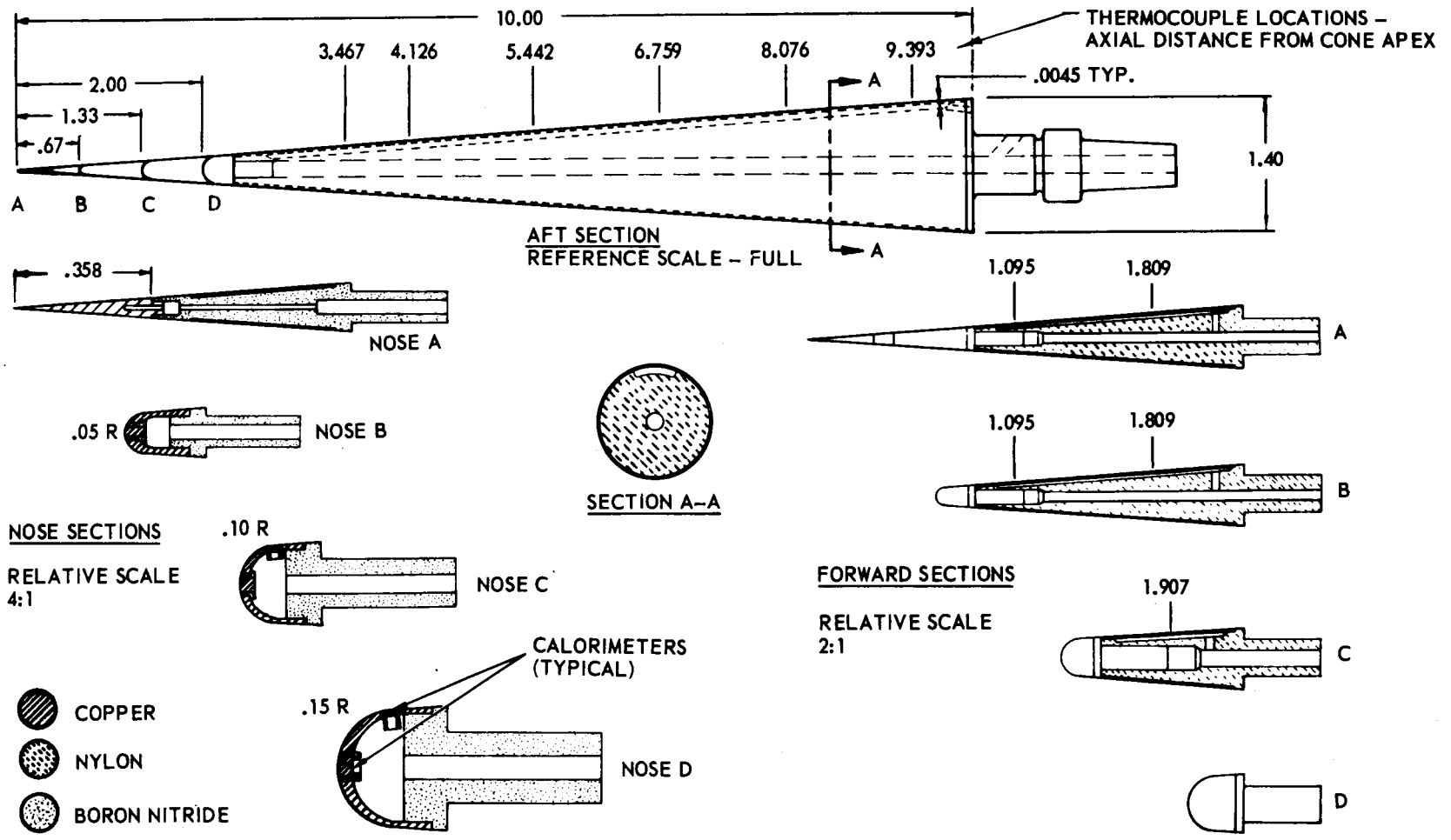

FIGURE 2 LTV HYPERVELOCITY WIND TUNNEL TEST 34 HEAT TRANSFER MODEL

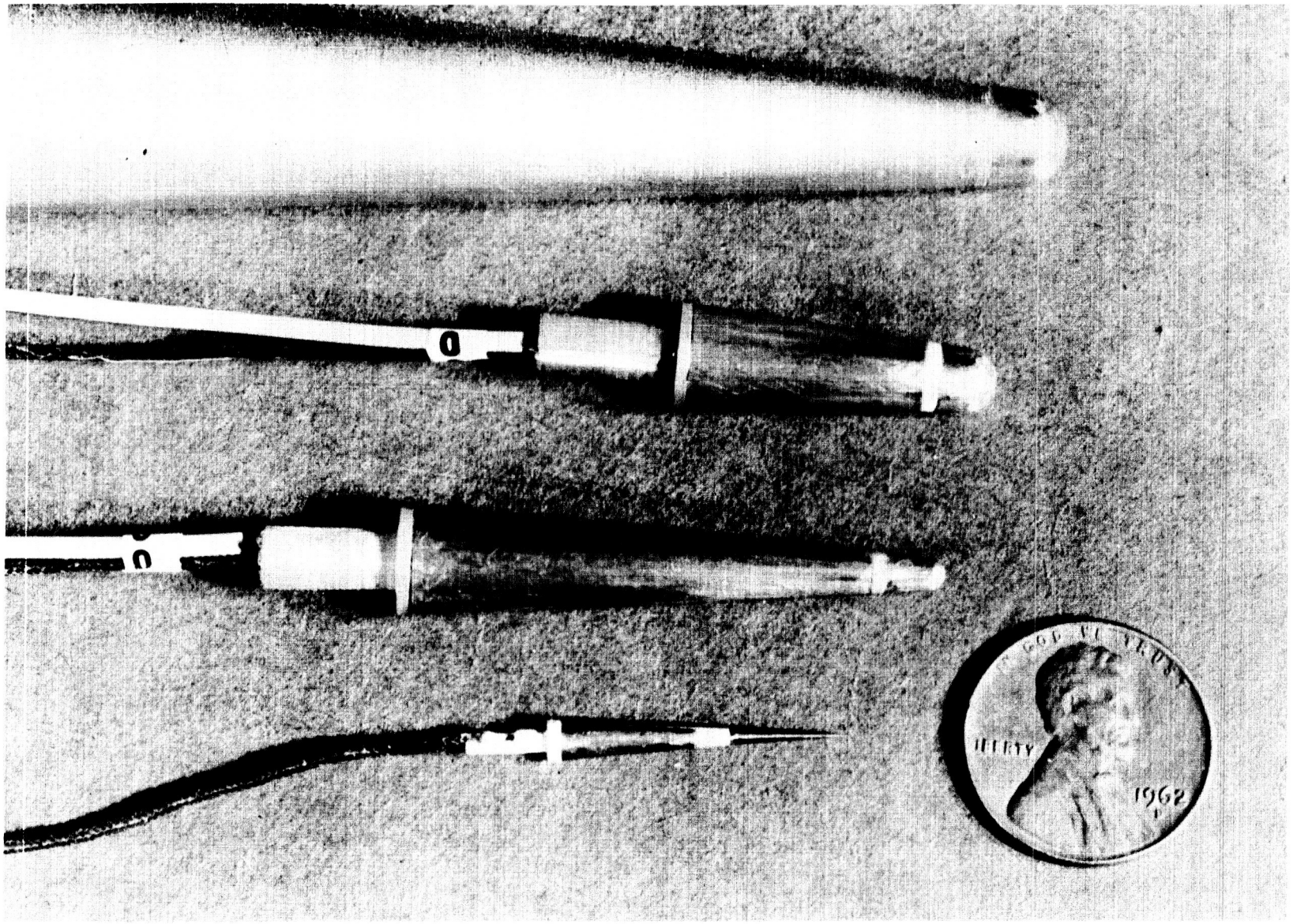

FIGURE 3 STAGNATION REGION DETAILS FOR HVWT MODELS

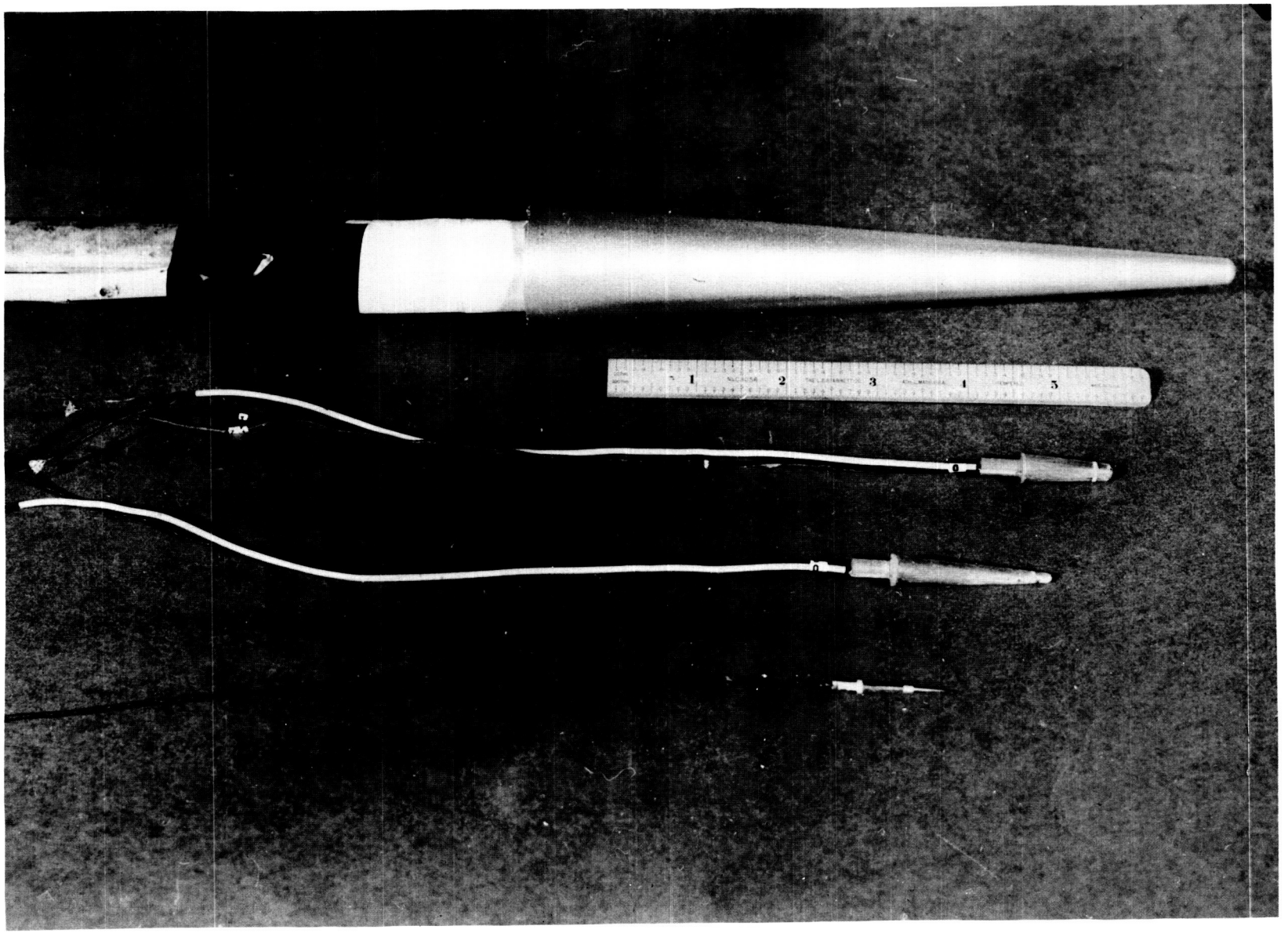

FIGURE 4 HVWT TEST MODELS

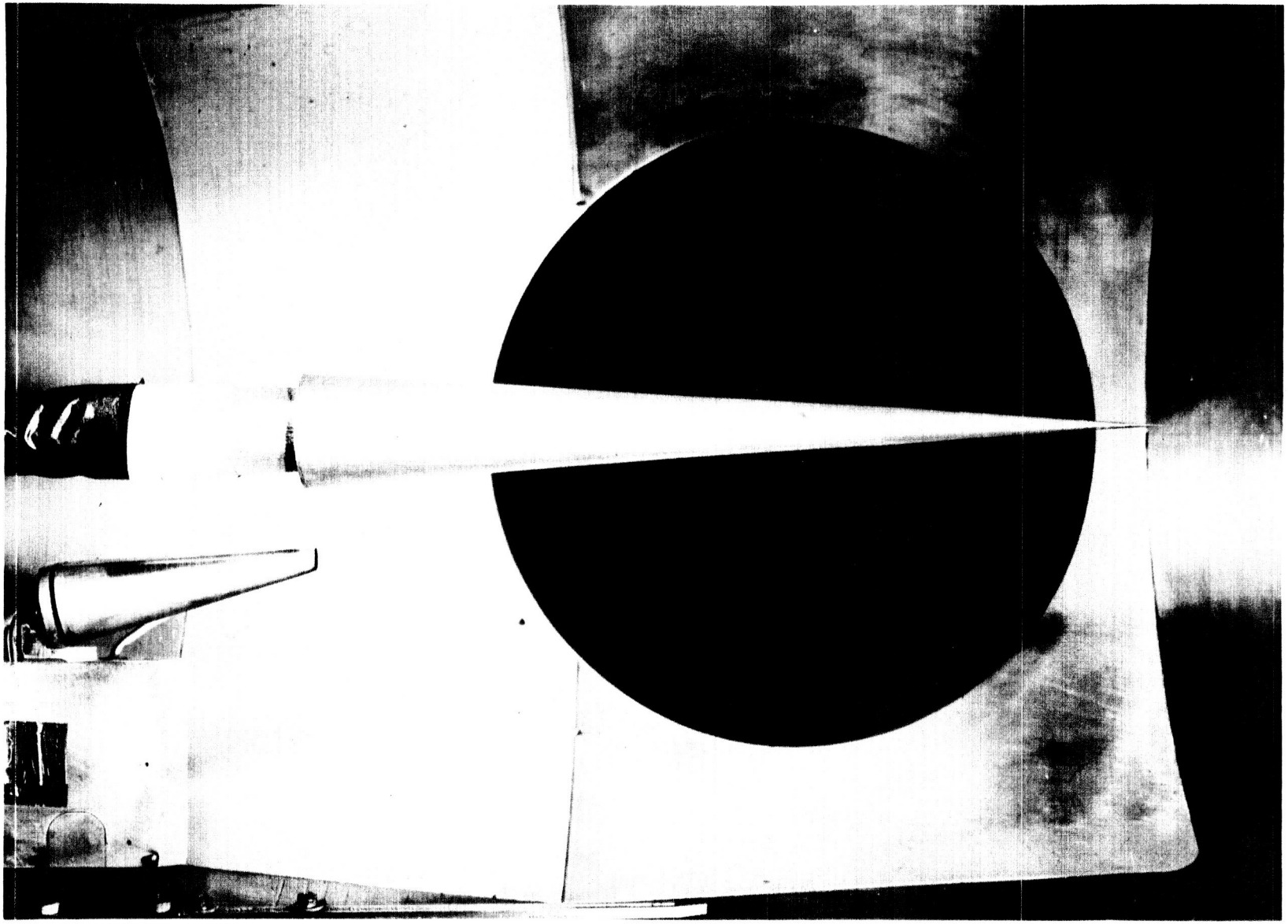

FIGURE 5 SHARP NOSED MODEL INSTALLED IN HVWT

3.0 DATA ANALYSIS

The data obtained in the plasma facility and in the hypervelocity wind tunnel are presented and compared to existing theories. The theoretical equations, together with various additional considerations, are discussed first, followed by the presentation of the data and by a comparison of the data with theory.

3.1 THEORETICAL EVALUATION OF HEATING RATES

The theoretical analysis of the data was based on the results of Fay and Riddell, Lees and Van Driest. A complete discussion of these expressions may be found in references 4, 5 and 6.

The real gas heating rates at the stagnation point of the spherically blunted cones was computed by

$$\dot{q}_{fs} = \frac{35.9}{\sqrt{R}} (\rho_s - \rho_\infty)^{.25} (\mu_s)^{.4} (\rho_s)^{.15} (\rho\mu)_w^{.1} (h_s - h_w), \qquad (1)$$

where the values and units are as defined in the list of symbols.

The heating distribution over the conical section of the spherically blunted models in both the plasma and HVWT tests were predicted on the basis of a Lees' distribution given by

$$\frac{\dot{q}_{vv}}{\dot{q}_{fs}} = \frac{A(\theta_c)\, S'/R}{[B(\theta_c) + (S'/R)^3]^{1/2}}, \qquad (2)$$

where

$$A(\theta_c) = \frac{\sqrt{3}}{2}\left[\left(1 - \frac{1}{\gamma_\infty M_\infty^2}\right)\sin^2\theta_c + \frac{1}{\gamma_\infty M_\infty^2}\right]^{1/2} \sqrt{\frac{\pi}{2} - \theta_c},$$

$$B(\theta_c) = \frac{3/16}{\sin^2\theta_c \left\{\left[1 - (1/\gamma_\infty M_\infty^2)\right]\sin^2\theta_c + (1/\gamma_\infty M_\infty^2)\right\}}$$

$$\times \left[\frac{D(\theta)}{\theta}\right]_{\theta = \frac{\pi}{2} - \theta_c} - \cot^3\theta_c,$$

and $$D(\theta) = (1 - 1/\gamma_\infty M_\infty^2)\left(\theta^2 - \frac{\theta \sin 4\theta}{2} + \frac{1-\cos 4\theta}{8}\right) + (4/\gamma_\infty M_\infty^2)\left(\theta^2 - \theta \sin 2\theta + \frac{1-\cos 2\theta}{2}\right) + \cdots .$$

The predicted values of the heating to the sides of the sharp-nosed models were based upon the Van Driest method as applied to the flat plate which was adjusted by the Mangler transformation to obtain the rates about the cone. The modified expression is

$$\dot{q}_w = \sqrt{3}\, S_t \rho_l u_l \left(h_l + P_r^{1/2} \frac{u_l^2}{2gJ} - h_w\right). \qquad (3)$$

3.2 PLASMA JET DATA

As discussed in Section 2.0, heating rate measurements were made on sharp and slightly blunted graphite models in the LTV Plasma Facility. The flow conditions and resultant experimental data are presented in Table I. As may be observed from this table, the heat transfer values obtained at the forward side calorimeter are only slightly different for models having a sharp nose and those having a nose radius of 0.065 inches. This is as expected because this position is a considerable distance aft of the nose, and one would expect the effects of nose radius to decrease as the distance away from the nose increases. This observation is further substantiated by the values obtained from the aft side calorimeter where all the values are essentially constant with the exception of the Model 1A value, which appears to be a bad data point. It should be pointed out that the mass loss data should be considered as approximate for the spherically blunted models because significant erosion occurred around the stagnation region as a result of the hole left by the calorimeter when it melted. The details of the nose region both before and after exposure to the plasma stream are presented in Figures 6 through 15. Figures 6 through 9 show the sharp pointed models which maintained a pointed configuration during the tests. The actual shape of the models before tests was conical, and the peculiar shape shown in the photographs being due to diffraction of the light around the point. The irregularities associated with the nose region of the spherically blunted models after exposure may be attributed to the previously mentioned erosion effects.

TABLE I

PLASMA TEST FLOW CONDITIONS

Model No.	Nose Radius (in.)	Stagnation Enthalpy (BTU/LB)	Heating rate to 3/4" flat face probe $\frac{BTU}{FT^2\ SEC}$	Mass Flow rate $\frac{LB}{MIN}$	Percent Oxygen	Recession (in.) Stagnation Point	Mass Loss (gms)	Exposure Time (Sec)	Heating rates to model calorimeters		
									Stag. Pt. $\dot{q}_1$	x=1.5in** $\dot{q}_2$	x=3.5in** $\dot{q}_3$
									($BTU/FT^2\ SEC$)		
1	Sharp	12,500	614	.1201	23.06	0.303	0.9930	51.0	--	392.8	203
1A	Sharp	12,500	578.3	.1196	23.11	0.360	1.0403	50.24	--	368	118
2	.05***	12,100	604.1	.1200	23.04	-----	-----	11.3*	2431	417	178
2A	.05***	13,500	669	.1197	23.14	0.121	1.0010	51.5	2583	429	198
3	.10	12,000	573.8	.1198	23.08	0.095	0.9849	50.1	2051	634	209
3A	.10	12,100	602	.1198	23.0	0.095	0.9850	50.0	2231	660	182.1

* Specimen was damaged during fabrication, and experienced structural failure after 11.32 sec.

** Distance measured from virtual tip on blunted models

*** .05 Nominal was measured as 0.065 after installation of stagnation calorimeters

NOTE: After exposure nose radius for the sharp models was measured as approximately 0.001, which appeared to be governed by graphite grain size.

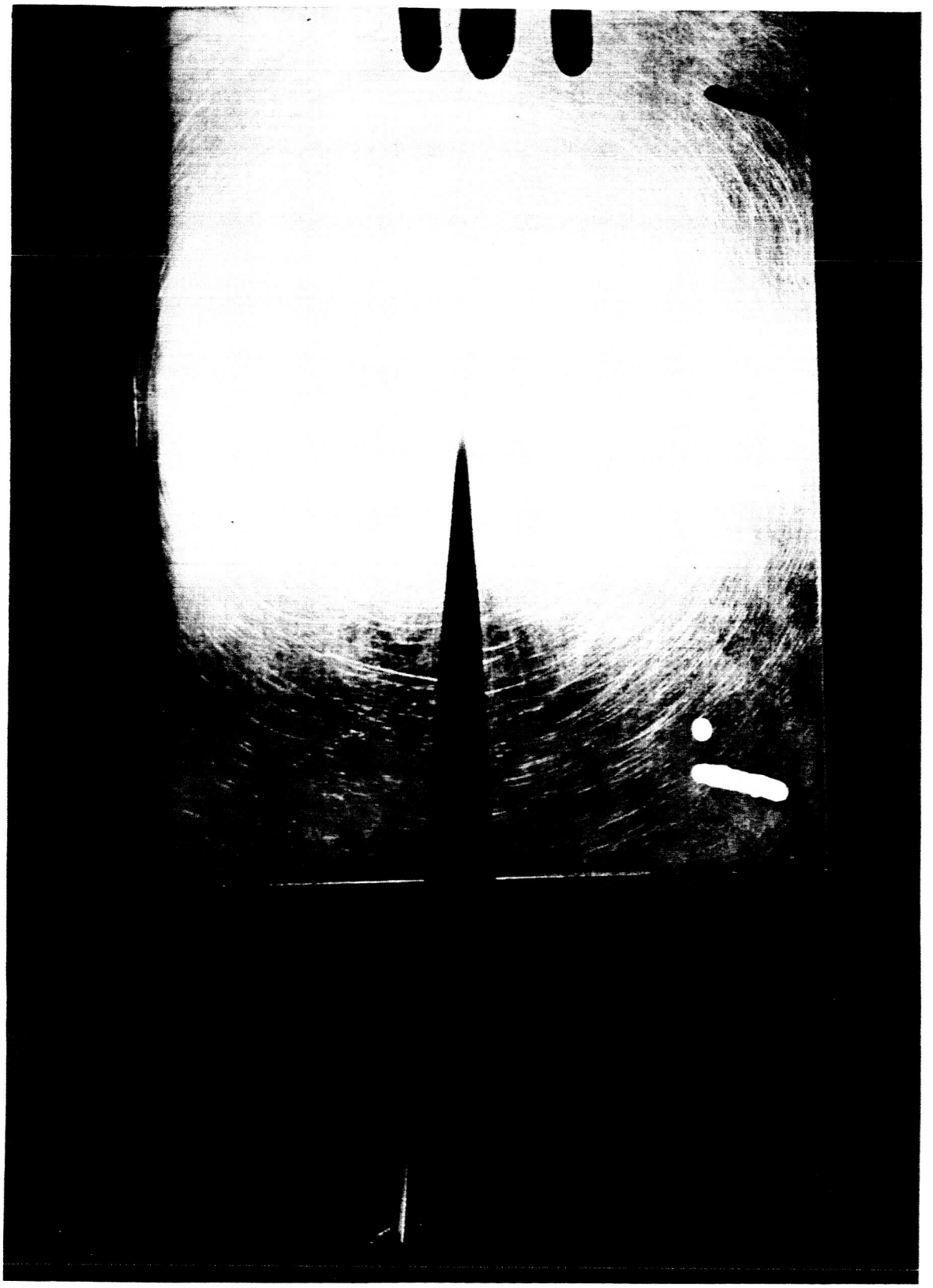

FIGURE 6 MODEL 1 BEFORE EXPOSURE

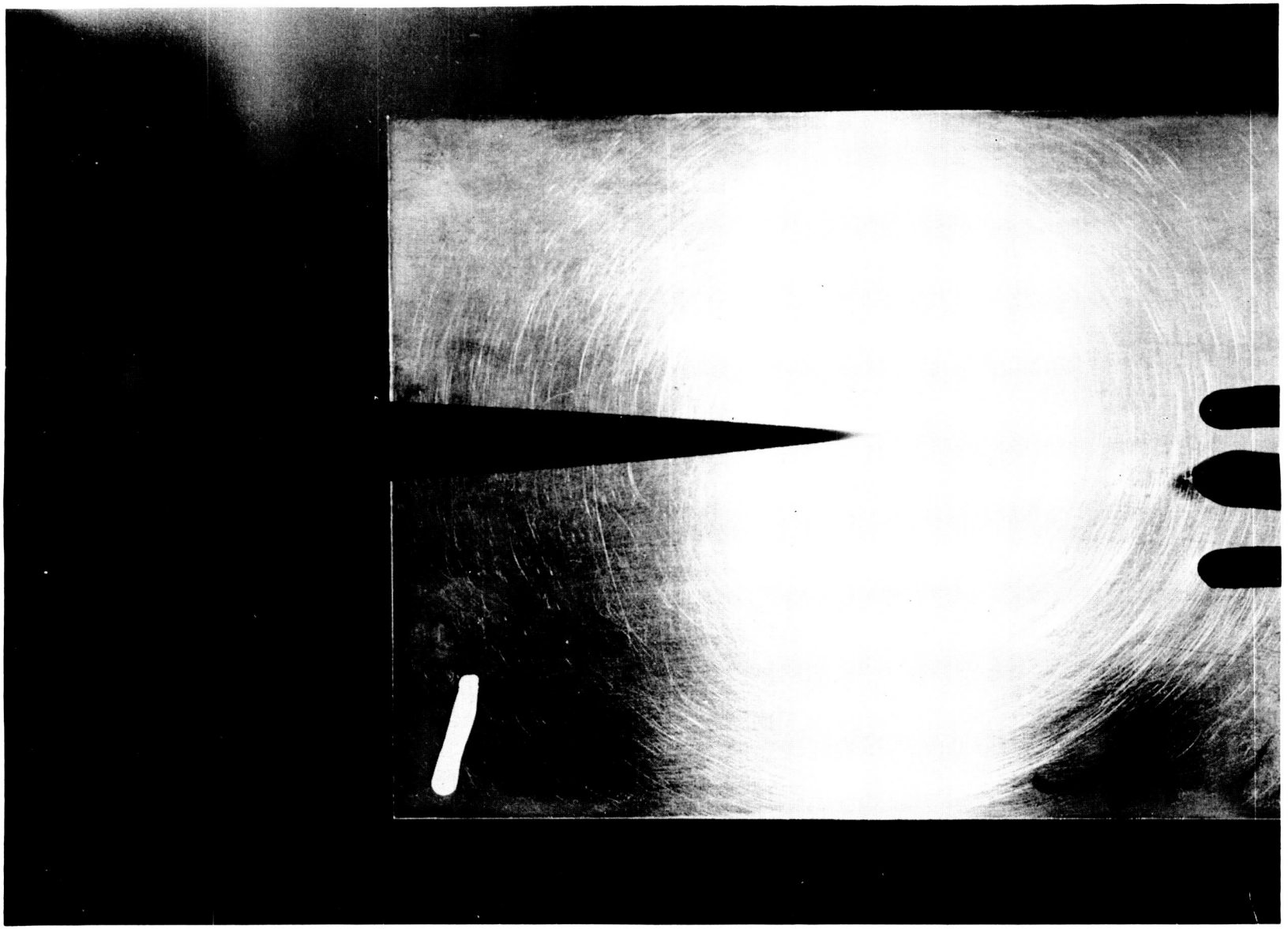

FIGURE 7 MODEL 1 AFTER 50 SECONDS EXPOSURE

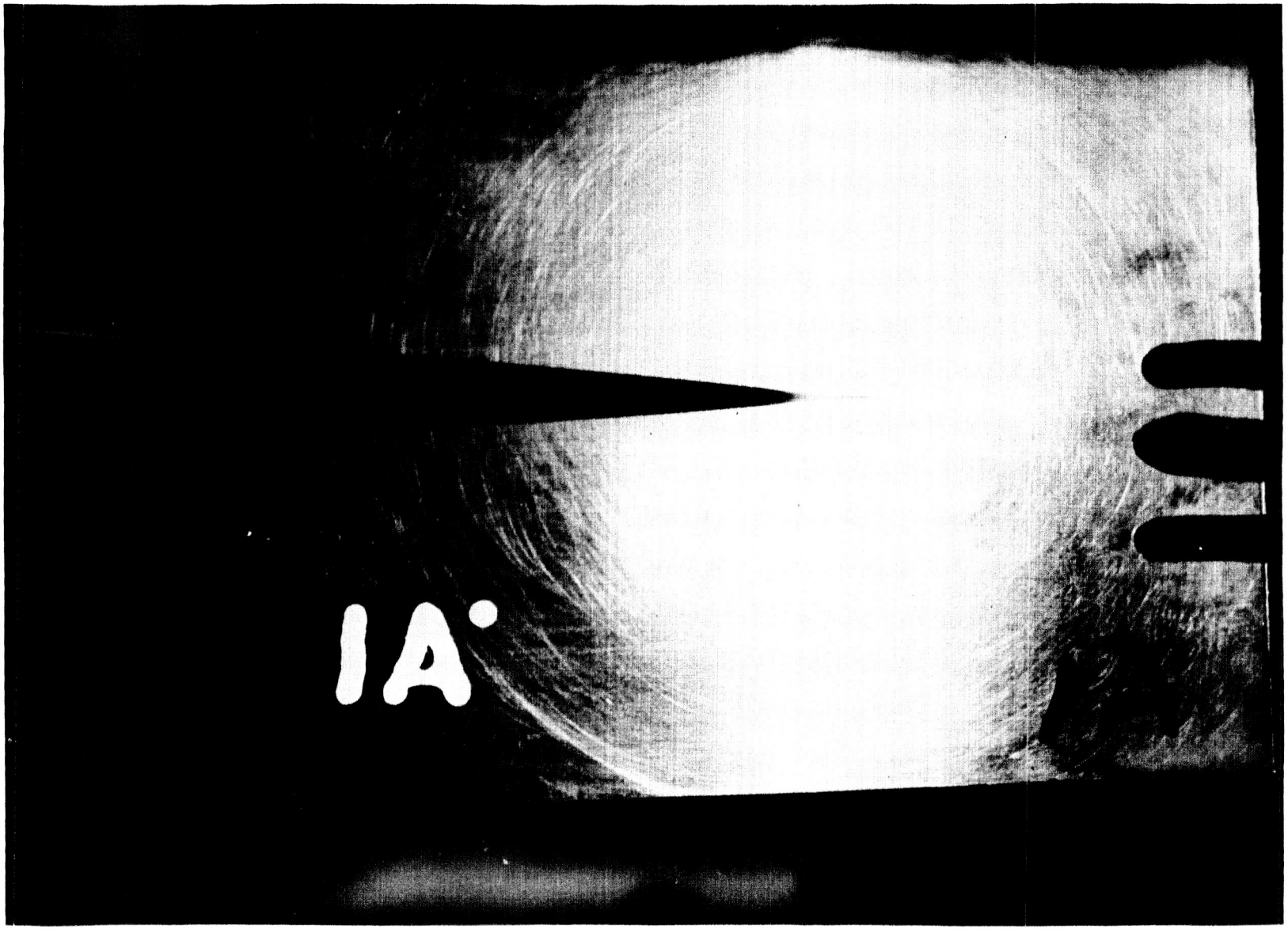

FIGURE 8 MODEL 1A BEFORE EXPOSURE

FIGURE 9 MODEL 1A AFTER 50 SECONDS EXPOSURE

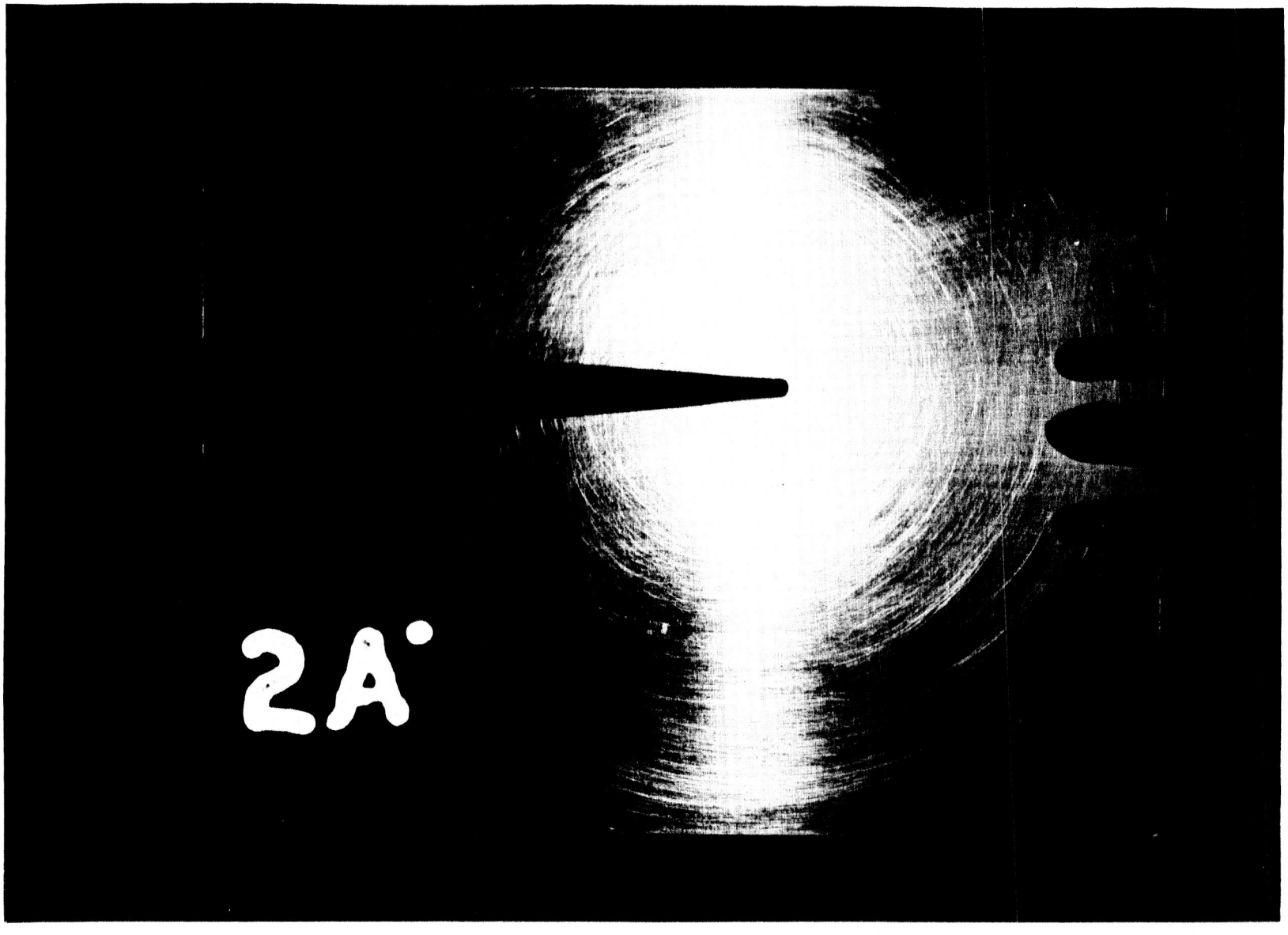

FIGURE 10 MODEL 2A BEFORE EXPOSURE

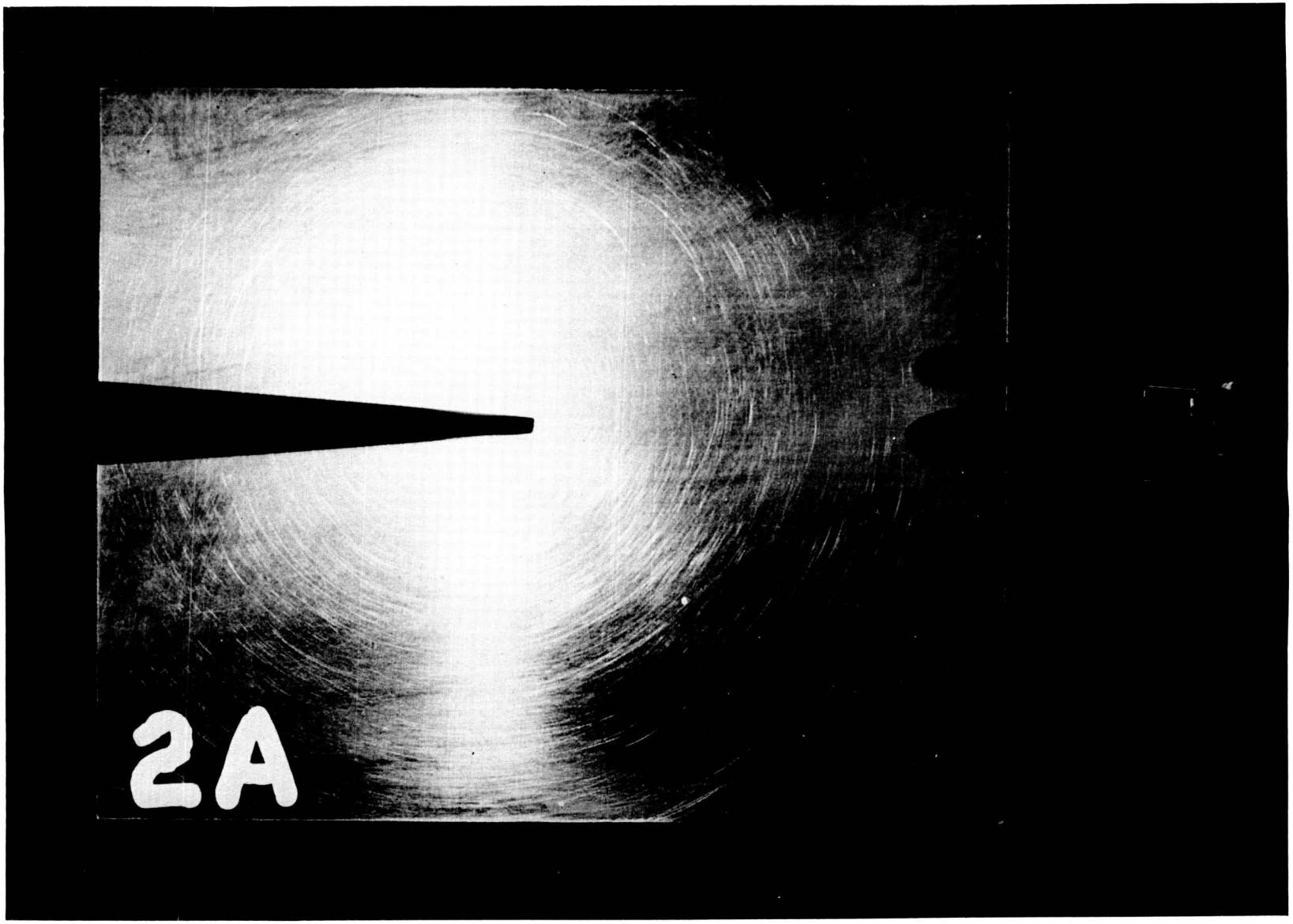

FIGURE 11 MODEL 2A AFTER 50 SECONDS EXPOSURE

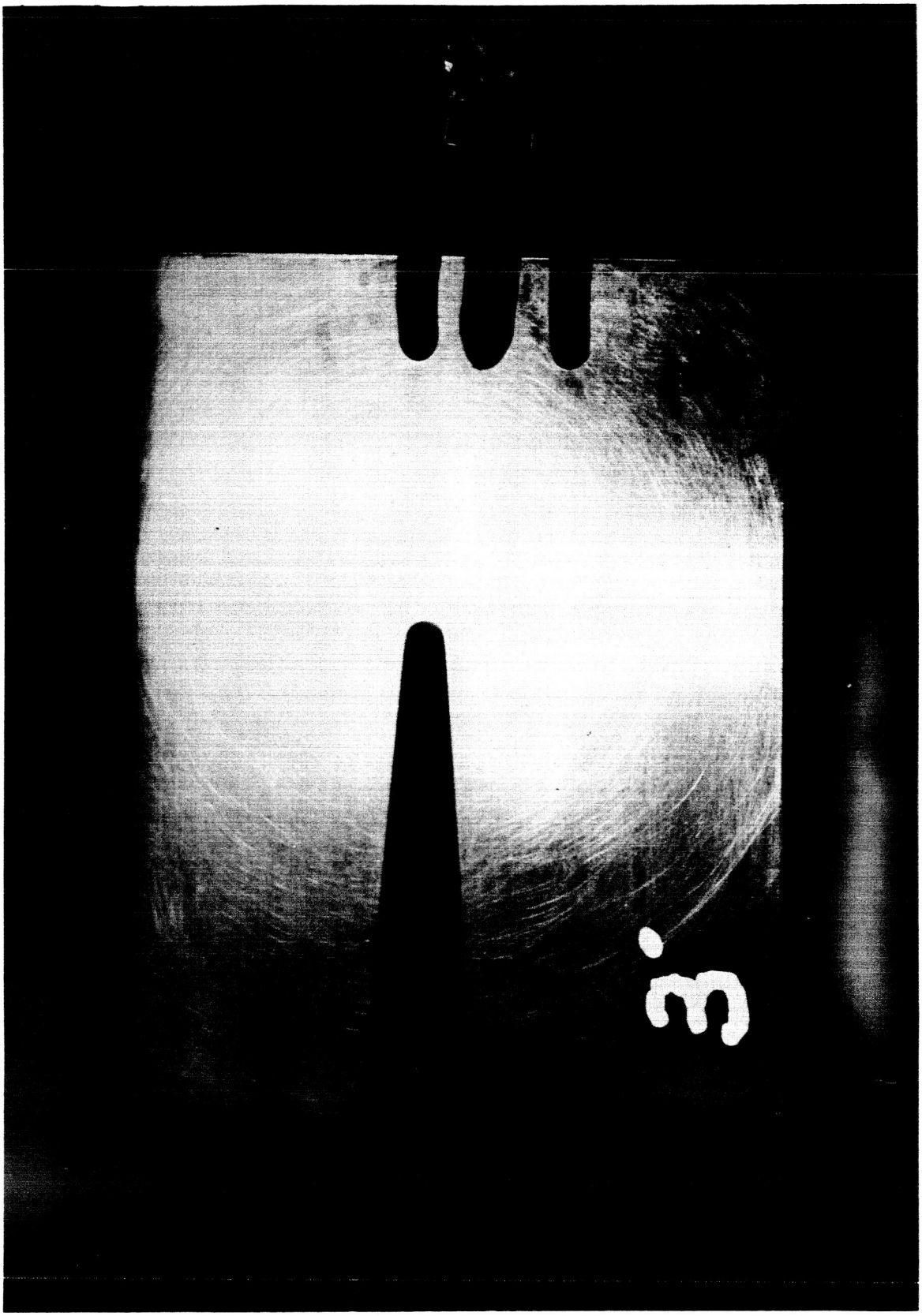

FIGURE 12 MODEL 3 BEFORE EXPOSURE

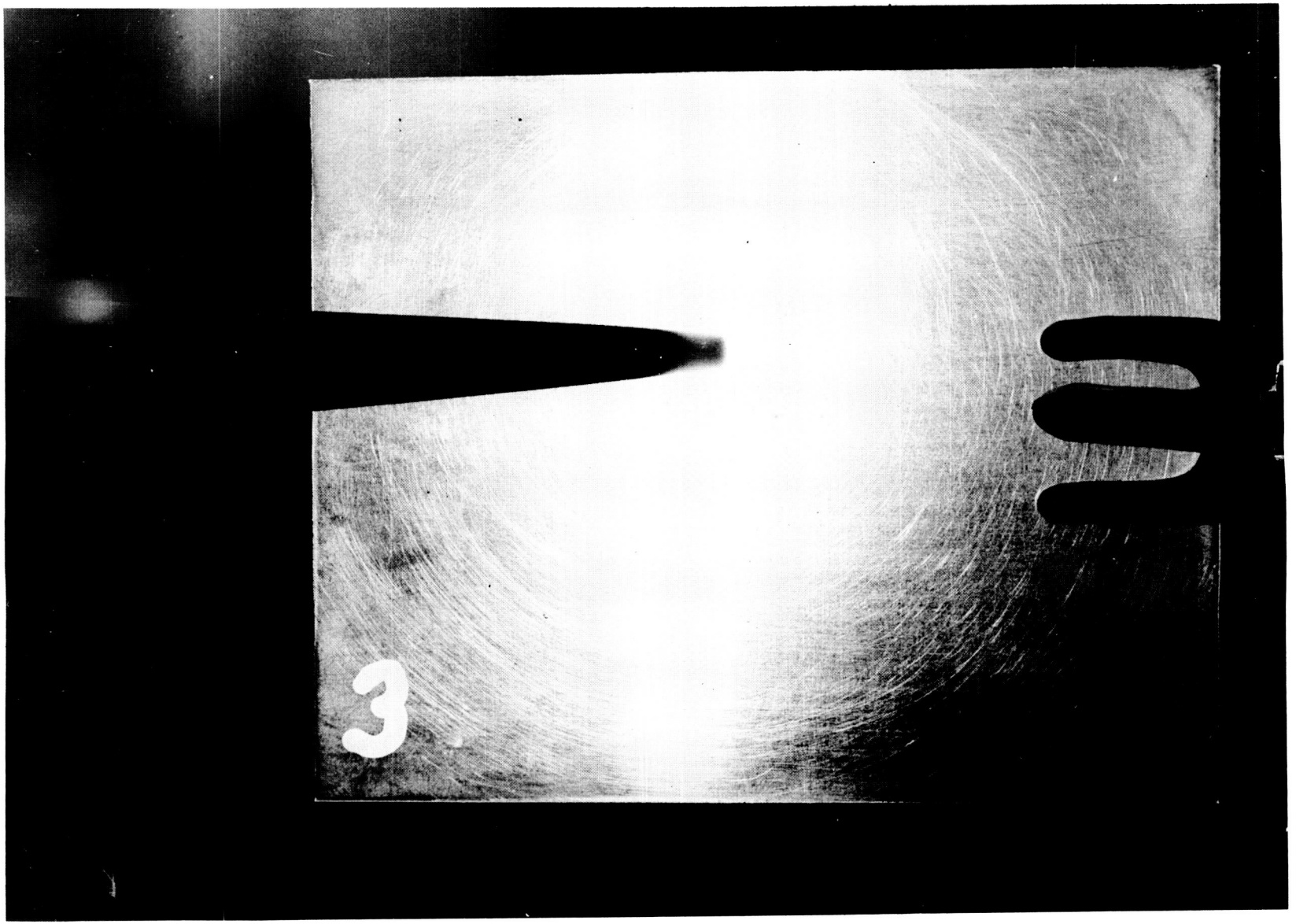

FIGURE 13 MODEL 3 AFTER 50 SECONDS EXPOSURE

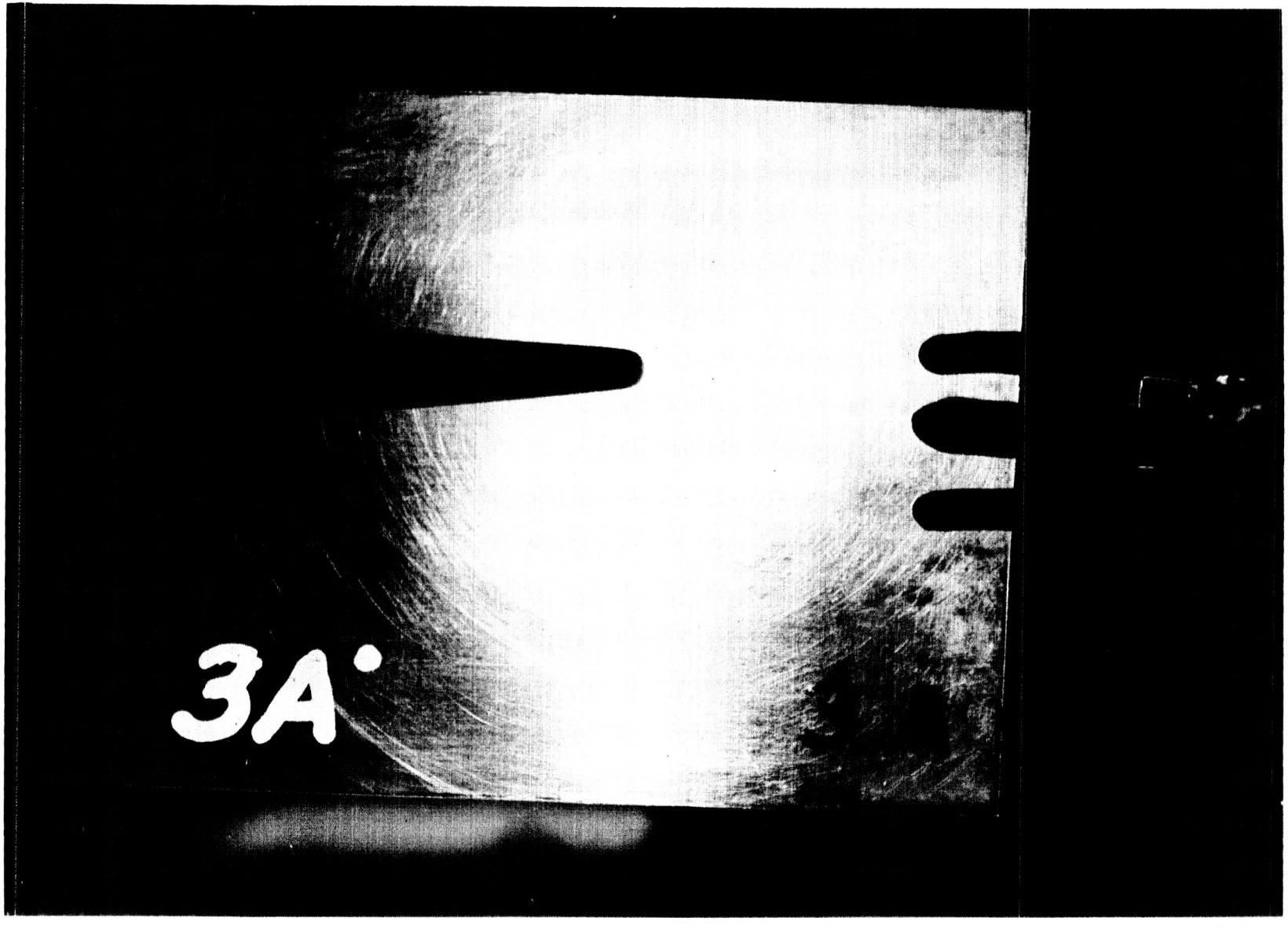

FIGURE 14 MODEL 3A BEFORE EXPOSURE

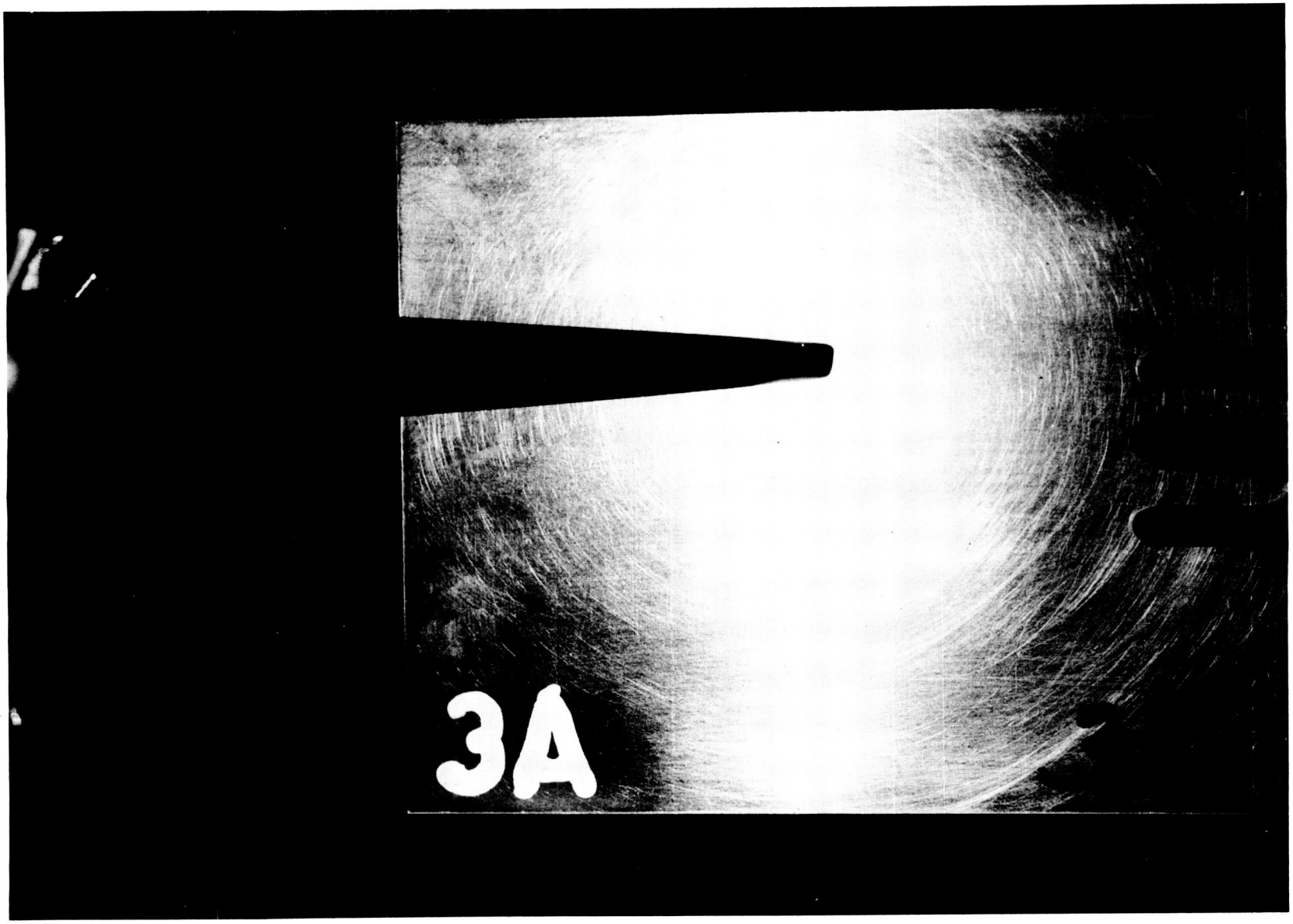

FIGURE 15 MODEL 3A AFTER 50 SECONDS EXPOSURE

3.2.1 Sharp Cone

The heating rates to the side of the graphite models were compared to the theory of Van Driest (Equation 3) and the results are shown in Figure 16. An investigation was made to evaluate the effects of viscous interaction, based on the work of Probstein (Reference 7). The viscous interaction effects upon the heat transfer rate was computed from the following expression,

$$\frac{\dot{q}_{fv}-\dot{q}_{fw}}{\dot{q}_{fw}} = \left\{\left[-.350 + .111\frac{T_w}{T_e} + (.429\gamma - .028)M_c^2\right] \times \frac{d_c F_1(K)\bar{x}_c}{\gamma M_c^2} + \left[.517 + .913\frac{T_w}{T_e} + .121(\gamma-1)M_c^2\right] \times \sqrt{(C/Re_x)_c}\Big/\sqrt{3}\tan\theta_c\right\},$$

where the terms on the right represent the induced pressure and transverse-curvature effects respectively. The effects of the viscous interaction parameter are shown as a dashed line in the figure. The deviations between the observed and predicted data are within the accuracy associated with the determination of the plasma properties. Some considerations of the stagnation point heating to the pointed model will be discussed in the following section.

3.2.2 Spherically Blunted Cone

The theoretical stagnation heating rates for the spherically blunted models were computed on the basis of the work of Fay and Riddell, (Equation 1). The experimental data was compared to the theory and the results are presented in Figure 17. The values have been non-dimensionalized with respect to the flat face calorimeter values to account for variations in enthalpy levels of the plasma stream and to compare the values on a common basis. Also shown in the figure are predicted values based upon the measured flat face calorimeter heating values. The flat face calorimeter values were scaled to model values by means of the following relation.

$$\dot{q}_s = \left(\dot{q}_{fCAL}/.637\right)\sqrt{.375/R} \quad . \qquad (4)$$

These values fall below the measured data indicating that the model was experiencing a higher stagnation enthalpy than was the calorimeter. Since the calorimeter indicates an average value, and gradients are known to exist in the plasma stream, the data appears quite reasonable.

Also shown in Figure 17, as Test #1, are heat transfer values which were deduced (by the method described in reference 1) from the mass loss data obtained by Medford and Holt. At the common points, reasonable agreement was obtained.

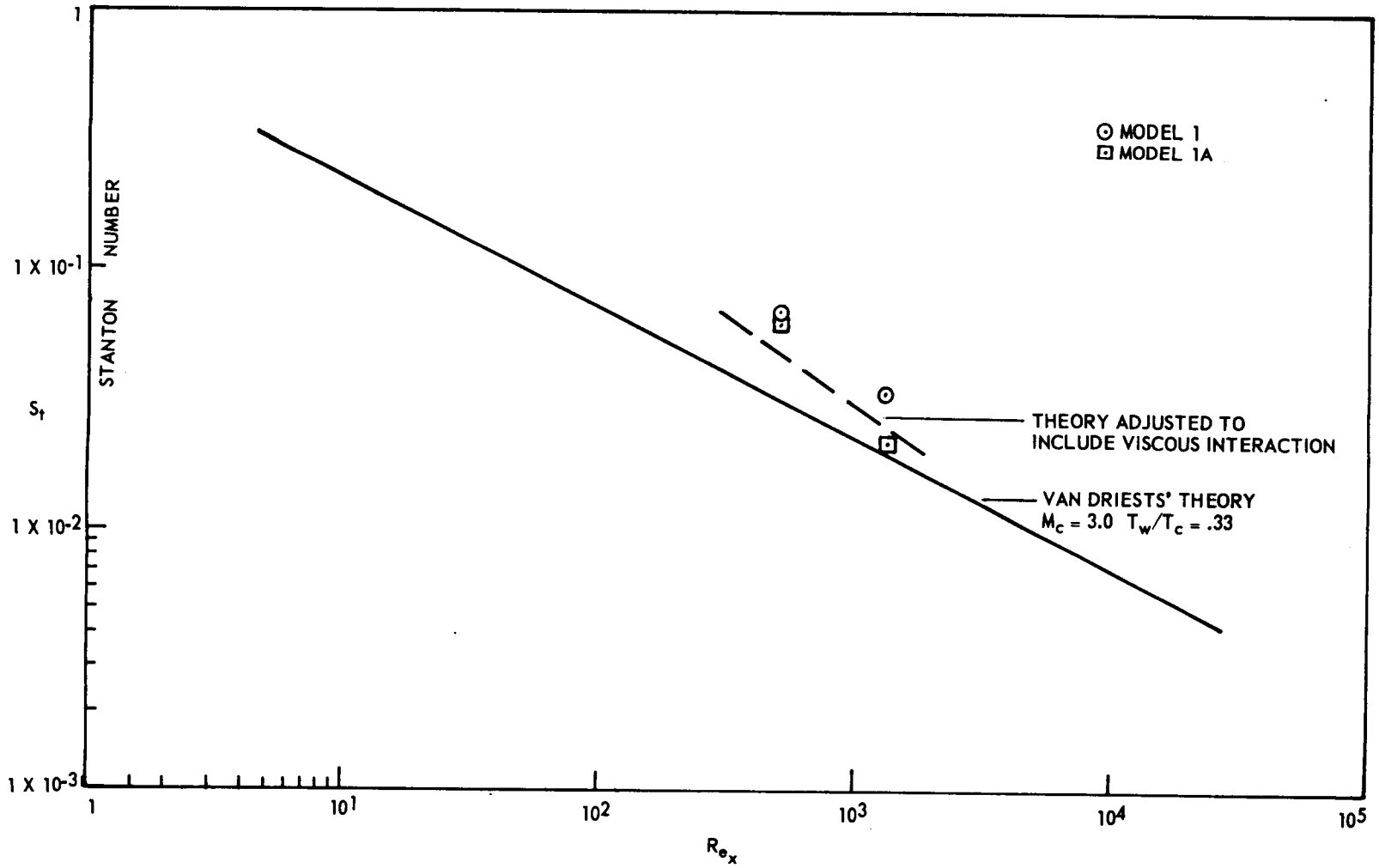

FIGURE 16 HEATING RATE TO SHARP POINTED CONES (PLASMA TEST)

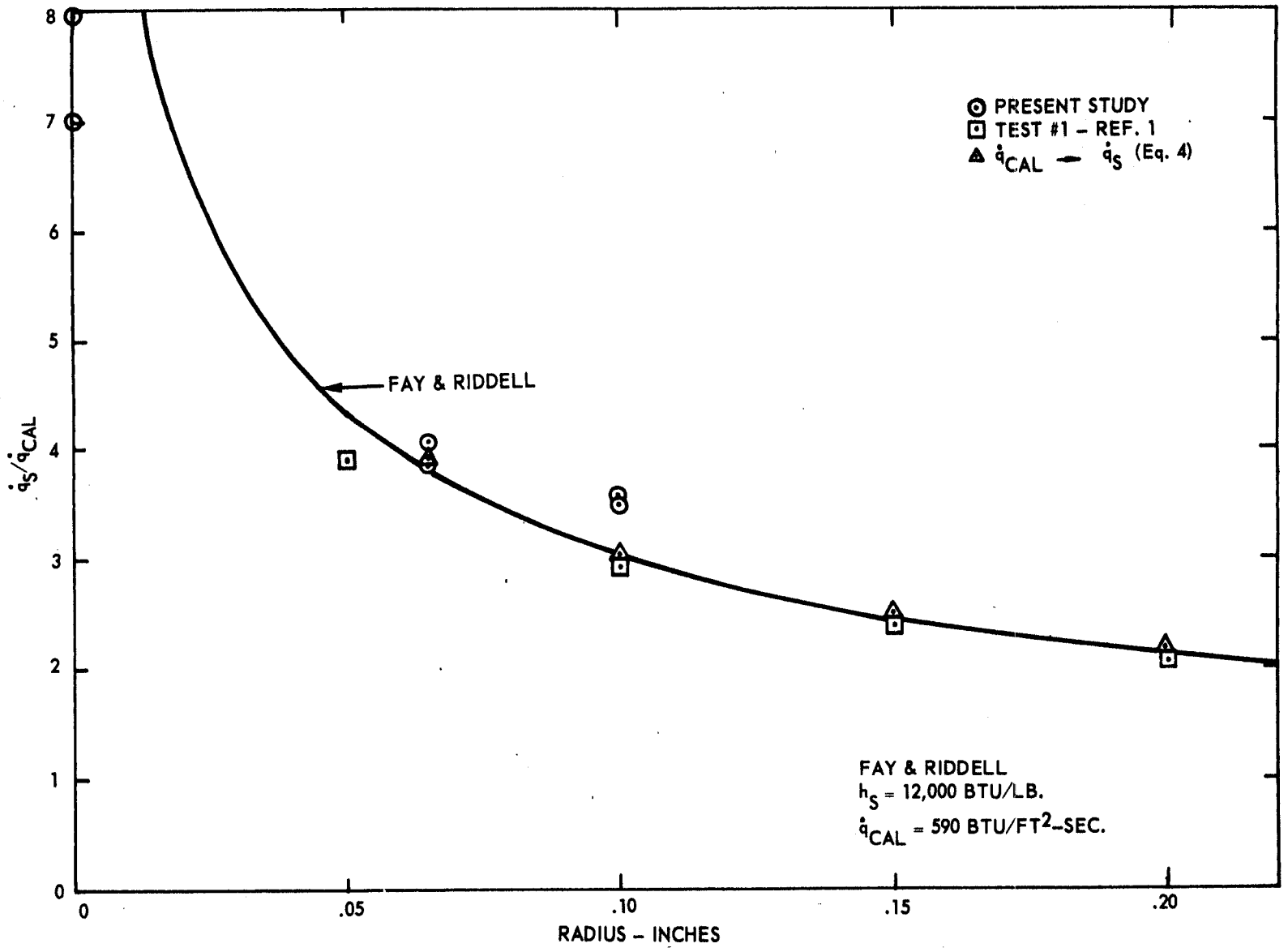

FIGURE 17 STAGNATION HEAT TRANSFER RATES FOR VARIOUS NOSE RADII (PLASMA TEST)

Heating values for the present test were deduced from the mass loss data at the stagnation point of the pointed models, and are presented in Figure 17 also. These values fall well below those predicted by the Fay & Riddell expression, necessitating an investigation of the limits of applicability of the theory. The pressure distribution which is embodied in the theory was assumed to fail when the nose radius became small compared to the mean free path, i.e. λ/R greater than approximately 0.01. For the plasma test, this condition corresponds to a nose radius of approximately 0.03 inches.

The heating distribution over the spherically blunted body was predicted on the basis of Lee's distribution (Equation 2), and the results are compared to the data in Figure 18. The theoretical values given by Equation 2 are not valid for S'/R less than approximately twenty since the static pressure near the tangent point is known to deviate markedly from the Newtonian value upon which Lee's distribution is based. However, the heating ratio obtained at the shoulder for the 0.10 inch nose radius model is in reasonable agreement (20 percent) with the ratio of shoulder to nose recession given by Medford and Holt. The flagged data in the figure has been adjusted to account for viscous interaction effects. Admittedly, this procedure deviates from the norm of adjusting the theory, but this was done here due to the nature of the abscissa in Figure 18.

3.3 HYPERVELOCITY WIND TUNNEL HEAT TRANSFER DATA

3.3.1 Models and Test Conditions

As discussed in Section 2.0, heat transfer data was obtained in the HVWT on four conical models having a 4° cone half-angle. The model was constructed of a common base section and interchangeable nose sections. The nose radius of curvature of each of the four different nose sections is given below

Nose Section	Nose Radius (In.)
A	Sharp
B	0.05
C	0.10
D	0.15

Each model (each nose section attached to the common base section) was tested at three different test conditions. The test conditions corresponding to the various tunnel runs are tabulated in Table II. Runs 2, 3, 5, and 7 correspond to Schlieren studies made on sharp graphite models which will be discussed later. The measured temperature rises of the calorimeter and model skin at the various instrumented points were converted to heating rates by usual calorimeter techniques.

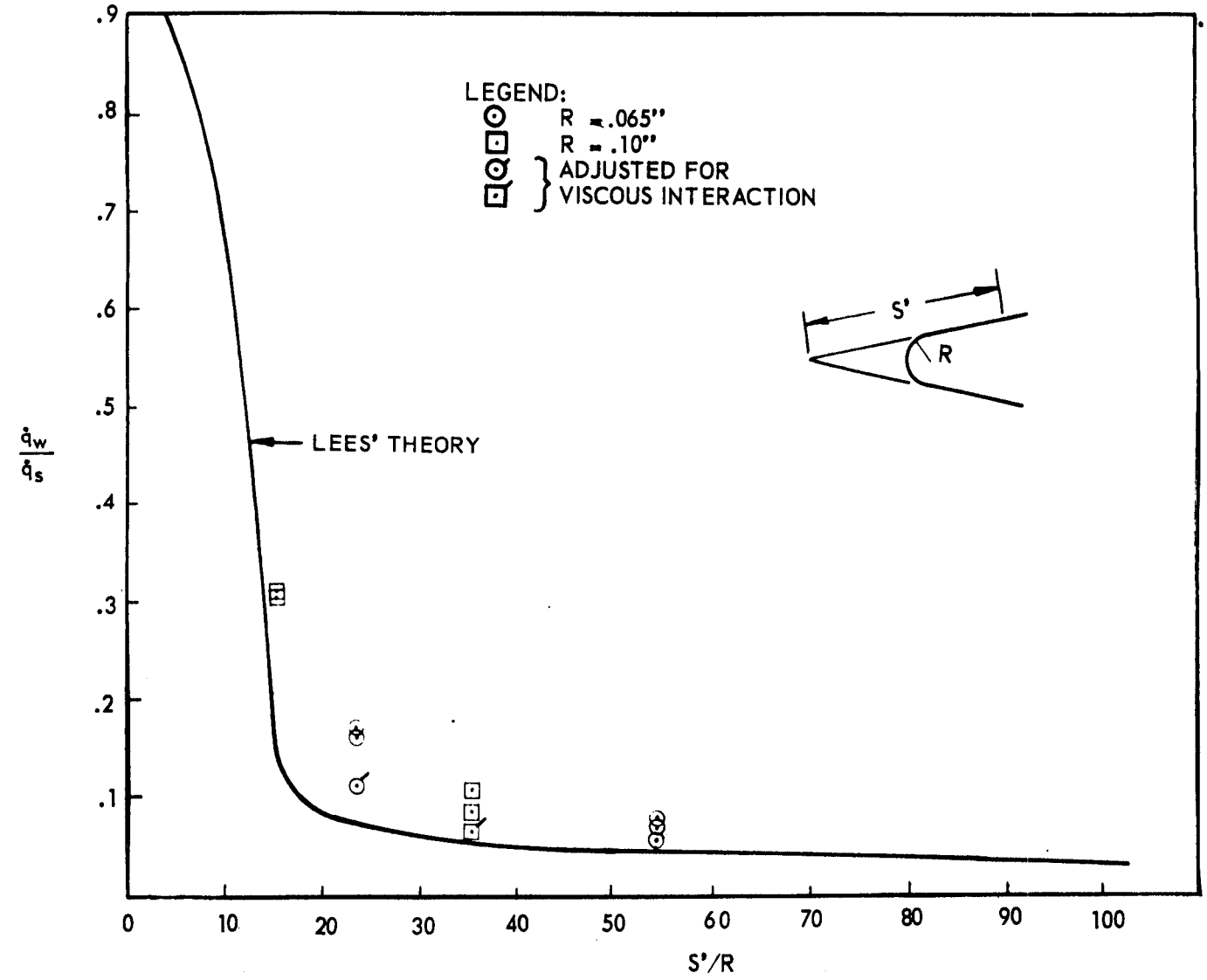

FIGURE 18 HEAT TRANSFER DISTRIBUTION OVER SPHERICALLY BLUNTED SLENDER CONES (PLASMA TEST)

TABLE II

HVWT FLOW CONDITIONS

Run Number	Nose Radius (inches)	Mach Number	(Reynolds No./Feet) X 10^{-6}	Total Enthalpy X 10^{-6} ft^2/sec^2	Static Pressure psia	Static Temp. ^oK	Total Pressure (After Normal Shock) psia
2*	sharp	17.30	1.123	24.556	.00727	36.0	2.840
3*	sharp	14.60	3.90	19.40	.00300	39.0	8.41
5**	sharp	14.66	3.899	19.380	.00302	39.4	8.408
7**	sharp	17.52	1.018	24.323	.00677	34.9	2.708
9	sharp	17.90	1.040	24.188	.005920	33.2	2.471
11	sharp	16.64	.146	44.783	.002429	71.2	.876
13	sharp	14.55	3.304	19.253	.02755	39.7	7.598
15	.05	14.46	3.203	18.537	.02590	38.7	7.056
16	.05	17.19	.881	27.793	.006961	41.4	2.680
17	.05	17.25	.128	42.559	.001786	63.0	.691
19	.10	17.44	.130	45.386	.001884	65.7	.746
20	.10	17.49	.941	25.622	.006271	36.9	2.499
21	.10	14.54	3.154	18.094	.02418	37.4	6.656

TABLE II
(Continued)

HVWT FLOW CONDITIONS

Run Number	Nose Radius (inches)	Mach Number	(Reynolds No./Feet) X 10^{-6}	Total Enthalpy X 10^{-6} ft^2/sec^2	Static Pressure psia	Static Temp. ^oK	Total Pressure (After Normal Shock) psia
22	.15	14.60	3.141	18.536	.02453	38.0	6.809
23	.15	17.67	.928	25.294	.005884	35.6	2.394
24	.15	17.73	.135	40.962	.001643	57.6	.670

* Graphite model before conditioning in Plasma Jet (Schlieren only)

** Graphite model after conditioning in Plasma Jet (Schlieren only)

3.3.2 Simulation Conditions

Before proceeding into a discussion of the heat transfer data obtained, it is interesting to determine the flight conditions actually simulated by the tunnel test conditions. This information, which is contained in Table III for the nominal tunnel conditions, was obtained by determining the flight altitude at which the tunnel Reynolds number per foot would occur for the given tunnel Mach number. Similar information for the plasma jet is also included in Table III. It can be seen that the HVWT can simulate rather low altitude flight at hypersonic Mach numbers.

3.3.3 Experimental Data

The experimental heating data obtained from the HVWT tests is tabulated in Table IV. For purposes of comparing the experimental results with theoretical values, it is convenient to discuss the sharp cone and blunted cone results separately, since different theoretical relations are applied in the two cases. Consequently, the experimental data obtained on the sharp cones will be discussed first, followed by a discussion of the blunted cone results.

3.3.3.1 Sharp cone.- The heat transfer data obtained on the sharp cone is compared with theory in Figures 19a and 19b where the heating rates have been converted to local Stanton numbers and plotted versus local Reynolds number. Comparisons are made to the theory of Van Driest (Reference 6) with corrections applied to account for the effects of viscous interactions. The viscous interaction corrections were calculated by the method of Probstein (Reference 7). It can be seen that the data obtained along the side of the cone agrees well with the Van Driest theory when the viscous interaction effects are included. The flagged symbols in Figures 19a and b which are joined by a straight line correspond to data obtained from the solid tip calorimeter which is approximately 0.36 inches long. The calorimeter was drilled and a thermocouple was imbedded in the hole such that the thermocouple bead was approximately 0.25 inches from the tip. The heating rate indicated by the tip calorimeter is a mean value resulting from the heating distribution existing on the tip section. The flagged symbols to the right are based on a local Reynolds number evaluated at a point corresponding to two-thirds of the calorimeter length or 0.25 inch, whereas the flagged symbols to the left are based on one-fourth of the calorimeter length.

A continuum analysis for flow on the tip indicates a heating rate which varies inversely with the square root of the distance from the tip. The mean heating value (based on length) experienced by a calorimeter subjected to continuum flow would correspond to a distance approximately one-fourth of the tip length. The measured Stanton number for runs 9 and 11, when compared to this one-fourth length continuum value, is found to be considerably below the theoretical value. These data tend to indicate that at least a portion of the

TABLE III

EQUIVALENT ALTITUDE FOR FACILITY TEST CONDITIONS

Facility	Reynolds No/Ft	Total Enthalpy (Ft^2/Sec^2)	Mach Number	Equivalent Altitude (Feet)
Plasma Jet	4.5×10^3	30×10^6	3.0	180,000
HVWT	$.13 \times 10^6$	44×10^6	17.5	150,000
HVWT	1×10^6	25×10^6	17.5	110,000
HVWT	3×10^6	18×10^6	14.5	90,000

REF: ARDC 1959 Standard Atmosphere

TABLE IV

HVWT HEATING DATA
EXPERIMENTAL HEATING RATES - BTU/FT^2 SEC

RUN NO.	Stagnation Value	Tangent Value	DISTANCE FROM VIRTUAL TIP (INCHES) 1.095	1.809	1.907	3.467	4.126	5.442	6.759	8.067	9.393
9	10.21		5.60	4.08		2.68	2.28	2.01	1.74		1.44
11	10.30		6.87	5.13		3.53	3.05	2.35	2.34		1.77
13	11.27		6.04	4.35		2.70	2.69	2.27	1.68		1.37
15	258.23		6.60	3.32		2.41	2.58	2.19	1.70		1.49
16	260.83		5.90	3.49		2.46	2.24	2.01	1.76		1.49
17	366.14		7.26	5.30		3.26	3.29	2.89	2.55		1.90
19	228.35	20.00			7.27	3.95	3.21	2.83	2.67		2.23
20	165.71	15.52			4.89	2.42	2.14	1.79	1.64		1.32
21	169.05	16.21			4.47	2.20	1.89	1.59	1.56		1.35
22	123.74	10.54				2.37	2.04	1.55	1.31	.95	1.07
23	123.74	10.34				2 64	2.17	1.63	1.47	1.17	1.12
24	155.85	14.07				4.05	3.20	2.63	2.30	2.20	1.93

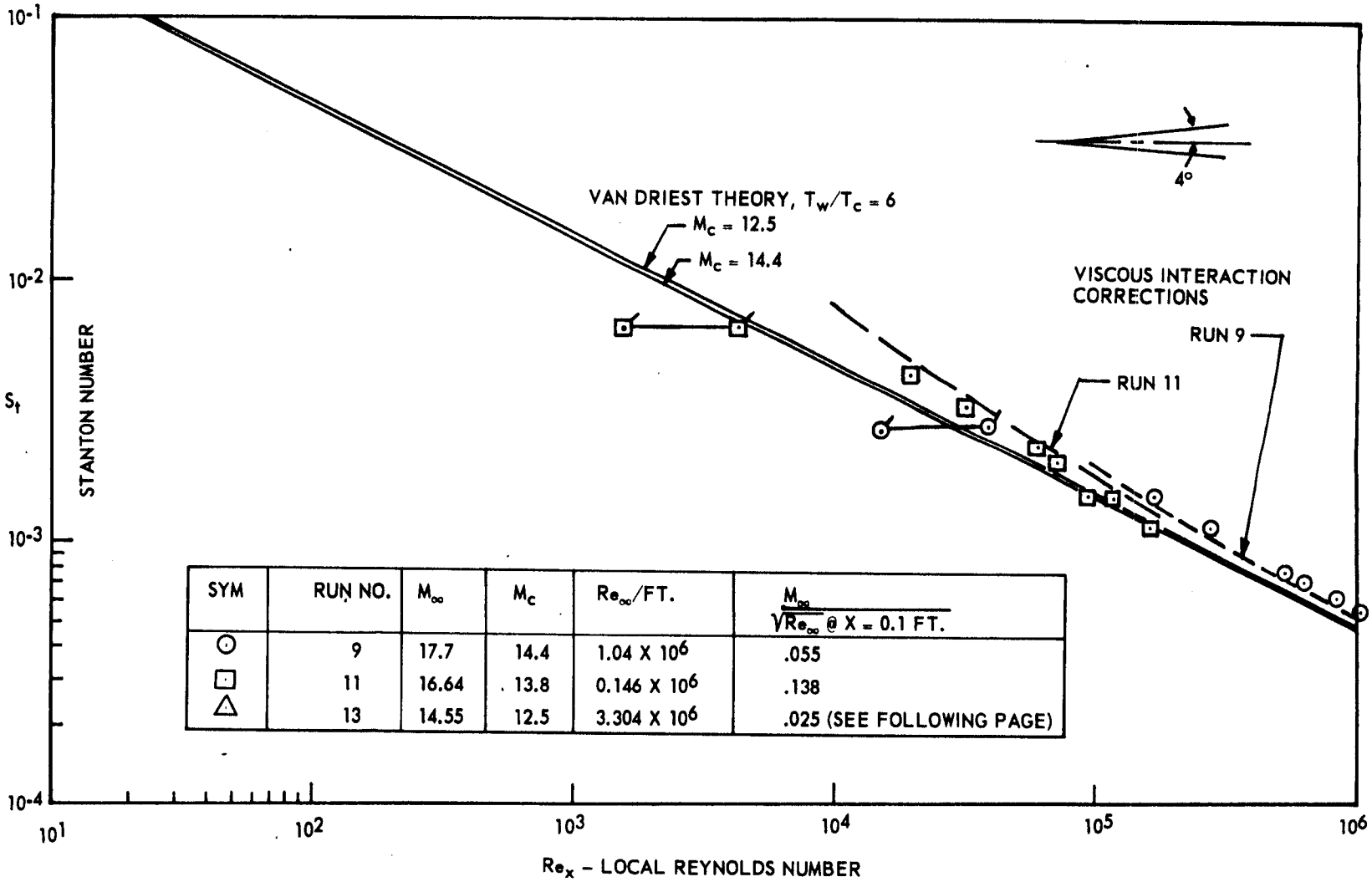

SYM	RUN NO.	M_∞	M_c	Re_∞/FT.	$\frac{M_\infty}{\sqrt{Re_\infty}}$ @ X = 0.1 FT.
⊙	9	17.7	14.4	1.04×10^6	.055
□	11	16.64	13.8	0.146×10^6	.138
△	13	14.55	12.5	3.304×10^6	.025 (SEE FOLLOWING PAGE)

FIGURE 19a HEAT TRANSFER DATA FROM HYPERVELOCITY WIND TUNNEL SHARP CONE

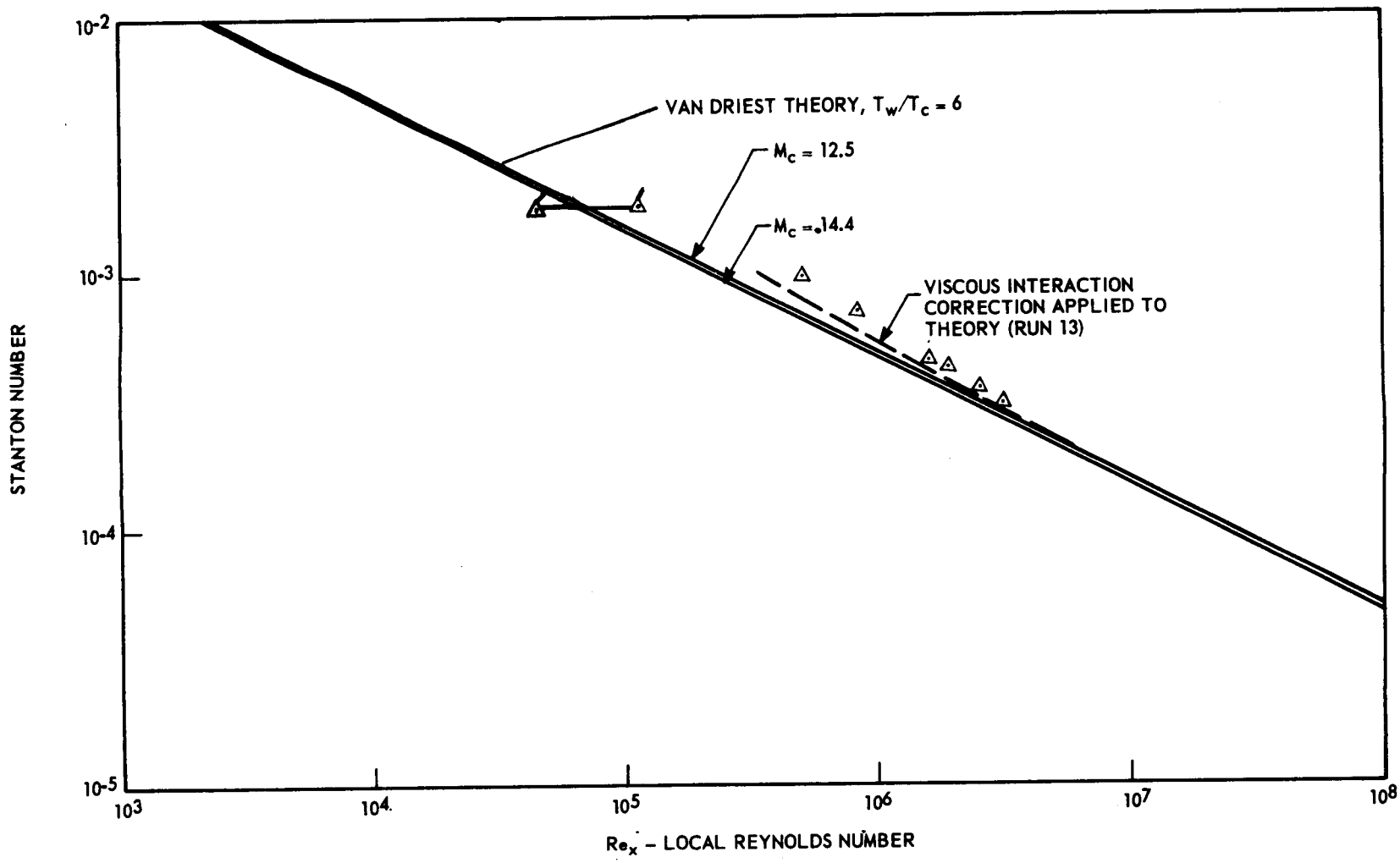

FIGURE 19b HEAT TRANSFER DATA FROM HYPERVELOCITY WIND TUNNEL SHARP CONE (CONTINUED)

tip calorimeter was in a slip flow regime for these test conditions. It also appears possible that run 13 experienced some slip effects although they would be expected to be less pronounced since a higher density and shorter mean free path exists for the flow conditions in run 13 as compared to runs 9 and 11. The parameter $M_\infty/\sqrt{R_\infty}$ shown on Figure 19a is indicative of the relative slip effects experienced by the calorimeter.

3.3.3.2 Spherically blunted cones.- The stagnation point heating rate data obtained on the spherically blunted cones was converted to an effective Nusselt number by means of the following relation

$$\tilde{N}_u \equiv \dot{q}_{fs} (C_p)_s R / k_s (h_s - h_w) \quad . \tag{5}$$

The results were plotted versus an effective Reynolds number given by

$$\tilde{N}_R \equiv \frac{\rho_s \sqrt{h_s}\, R}{\mu_s} \sqrt{\frac{P_s}{\rho_s h_s}} \quad . \tag{6}$$

This method of presentation offers a common basis for comparison of the experimental wind tunnel data obtained at various flow conditions with theory. The comparison is shown in Figure 20. The agreement is considered quite good, since deviations between theoretical and experimental values did not exceed 25 percent in any case.

The experimental heating distribution on the sides of the spherically blunted cones was normalized with respect to measured stagnation point values and compared to the theoretical distribution of Lees (Equation 2). The results are shown in Figures 21, 22, and 23 for nose radii of 0.05, 0.10, and 0.15 inch, respectively. It can be seen that reasonable agreement exists between the experimental data and the theoretical Lee's distribution for S'/R greater than twenty.

3.4 SCHLIEREN STUDIES

Studies were conducted in the HVWT to ascertain the extent of the interaction region between the boundary layer and shock wave, as well as to determine whether the shock was attached or detached. These studies were conducted both before and after the graphite model has been subjected to the total heat load predicted for a 45°re-entry down to 60,000 feet. The graphite model maintained its pointed configuration through the conditioning process, but some surface effects such as increased roughness were observed after conditioning.

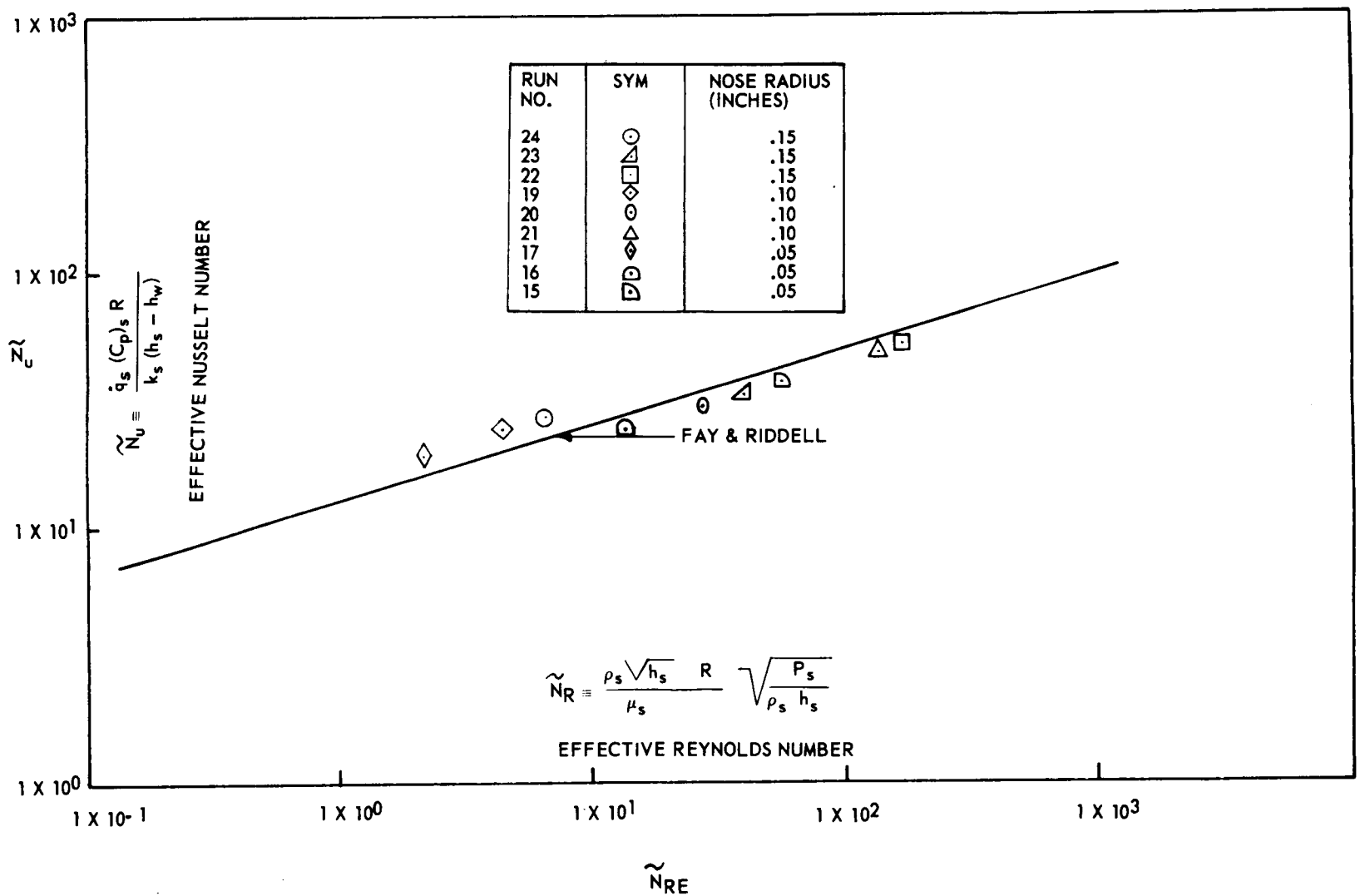

FIGURE 20 STAGNATION HEATING TO SPHERICALLY BLUNTED CONES – HVWT TESTS

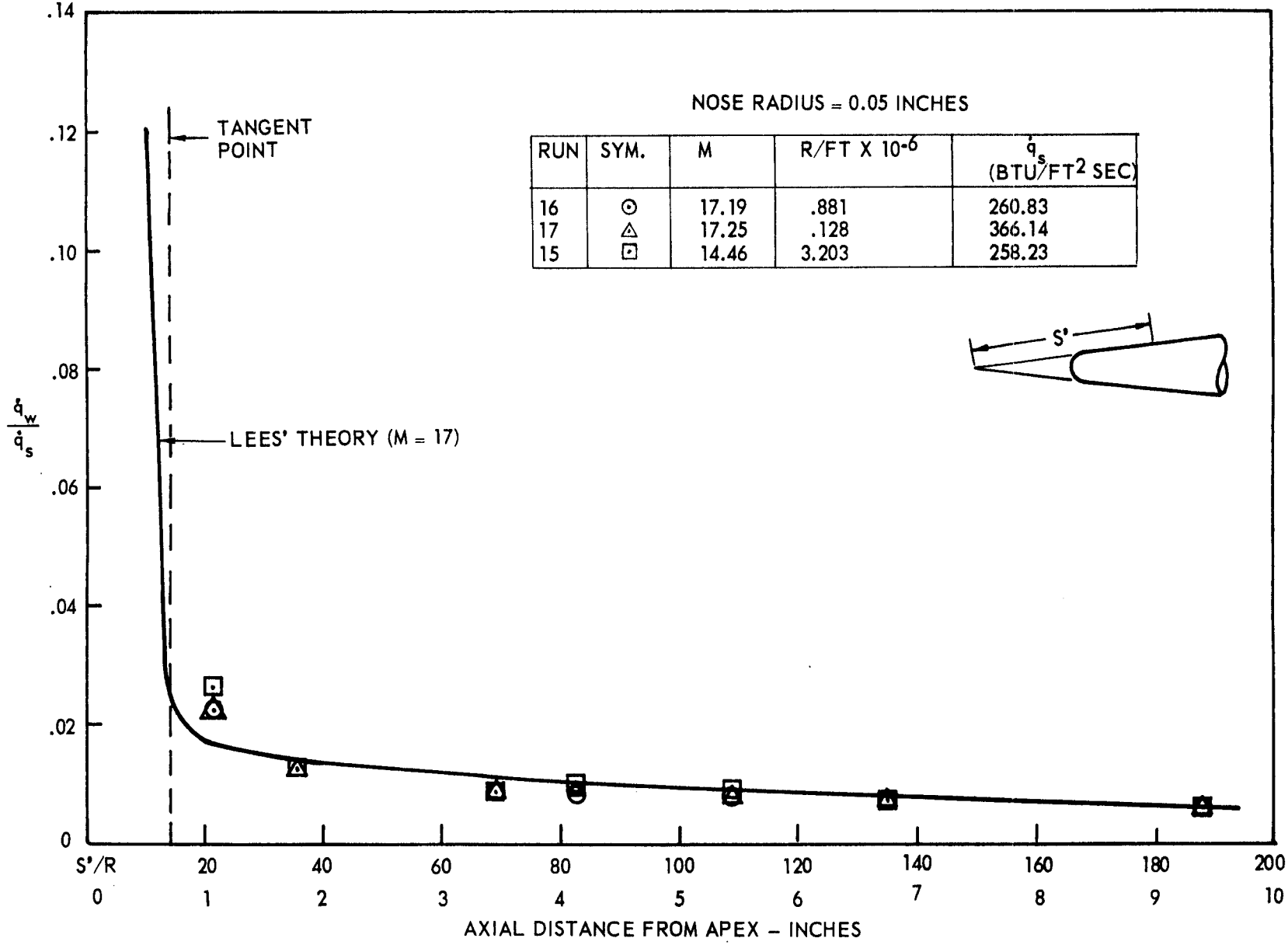

FIGURE 21 HEATING DISTRIBUTION OVER SPHERICALLY BLUNTED SLENDER CONES

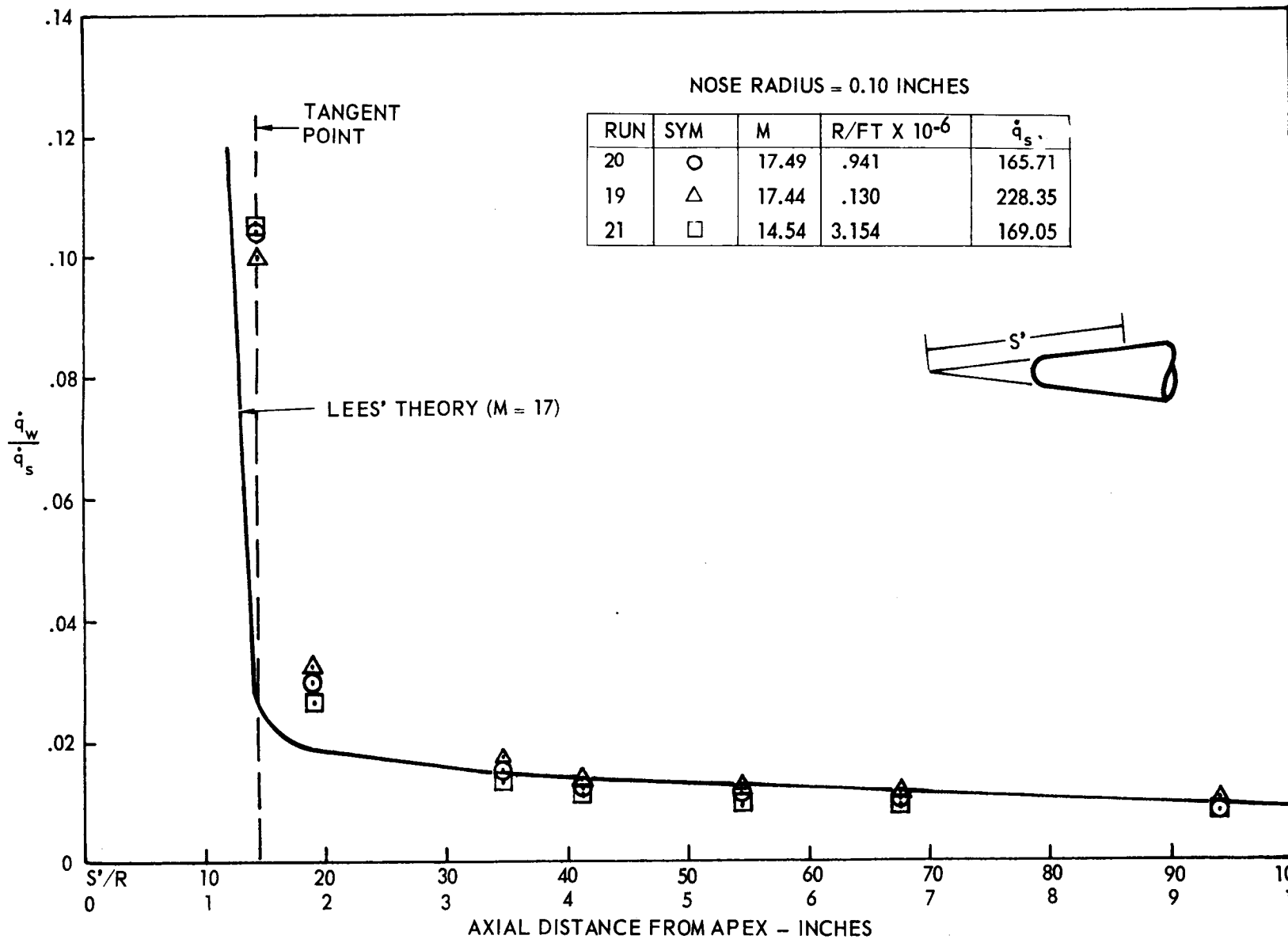

FIGURE 22 HEATING DISTRIBUTION OVER SPHERICALLY BLUNTED SLENDER CONES (CONTINUED)

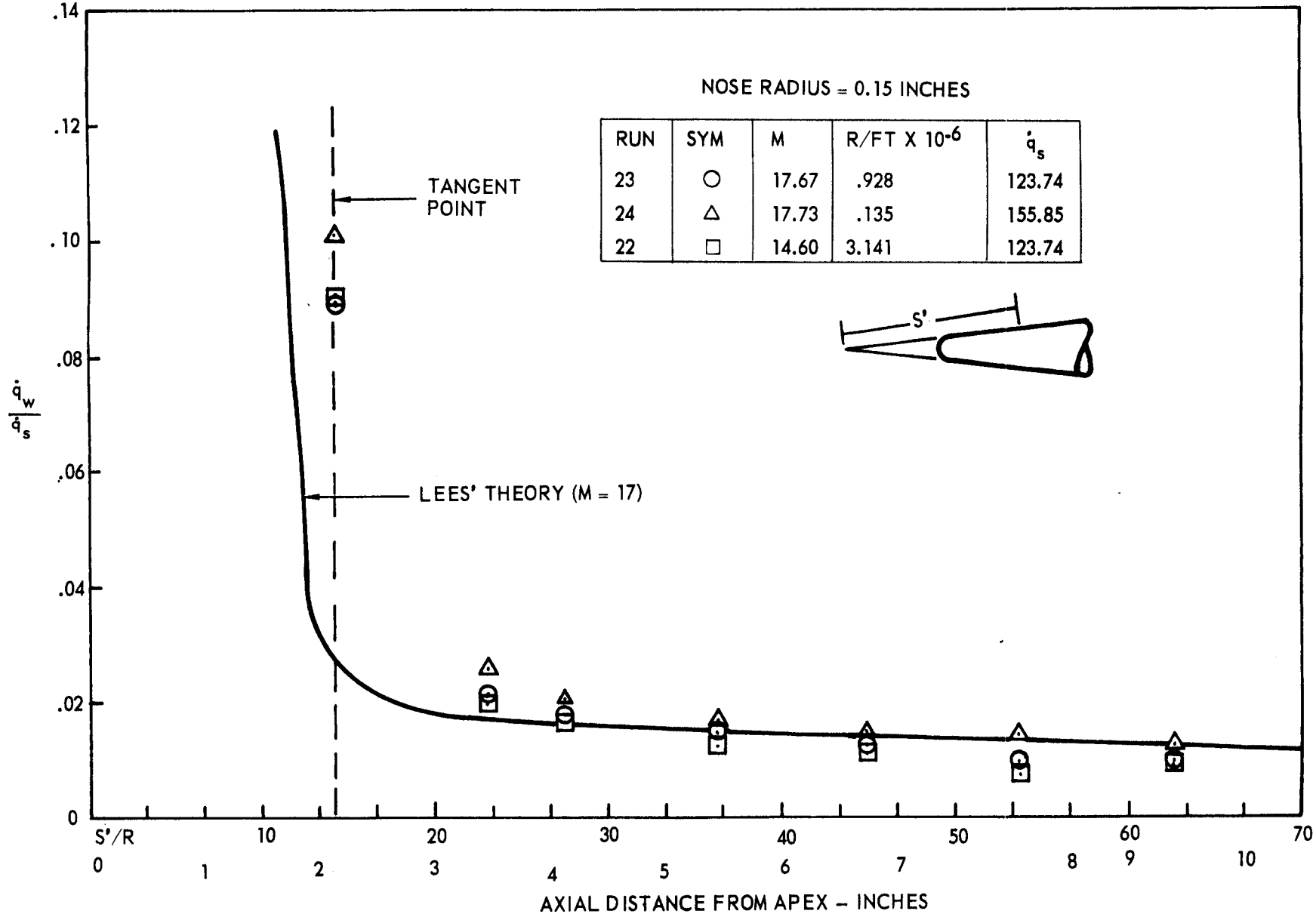

FIGURE 23 HEATING DISTRIBUTION OVER SPHERICALLY BLUNTED SLENDER CONES (CONTINUED)

The Schlieren photographs are presented in Figures 24 through 27. In each case, the boundary layer and shock front are clearly distinguishable in the region aft of the nose, but the shock was too weak near the nose to identify clearly. However, extrapolation from the aft section down to the tip tends to indicate an attached shock with a small interaction region aft of the tip. Figures 26 and 27 present data at higher Reynolds numbers, but lower Mach numbers, which tend to indicate similar results but with a smaller degree of interaction. In each case, the effects of conditioning were found to be minimal on the external flow field.

Figures 28 and 29 are Schlieren photographs of the flow field around the HVWT heat transfer model. They are included here to illustrate the effect of nose blunting on the boundary layer and shock pattern.

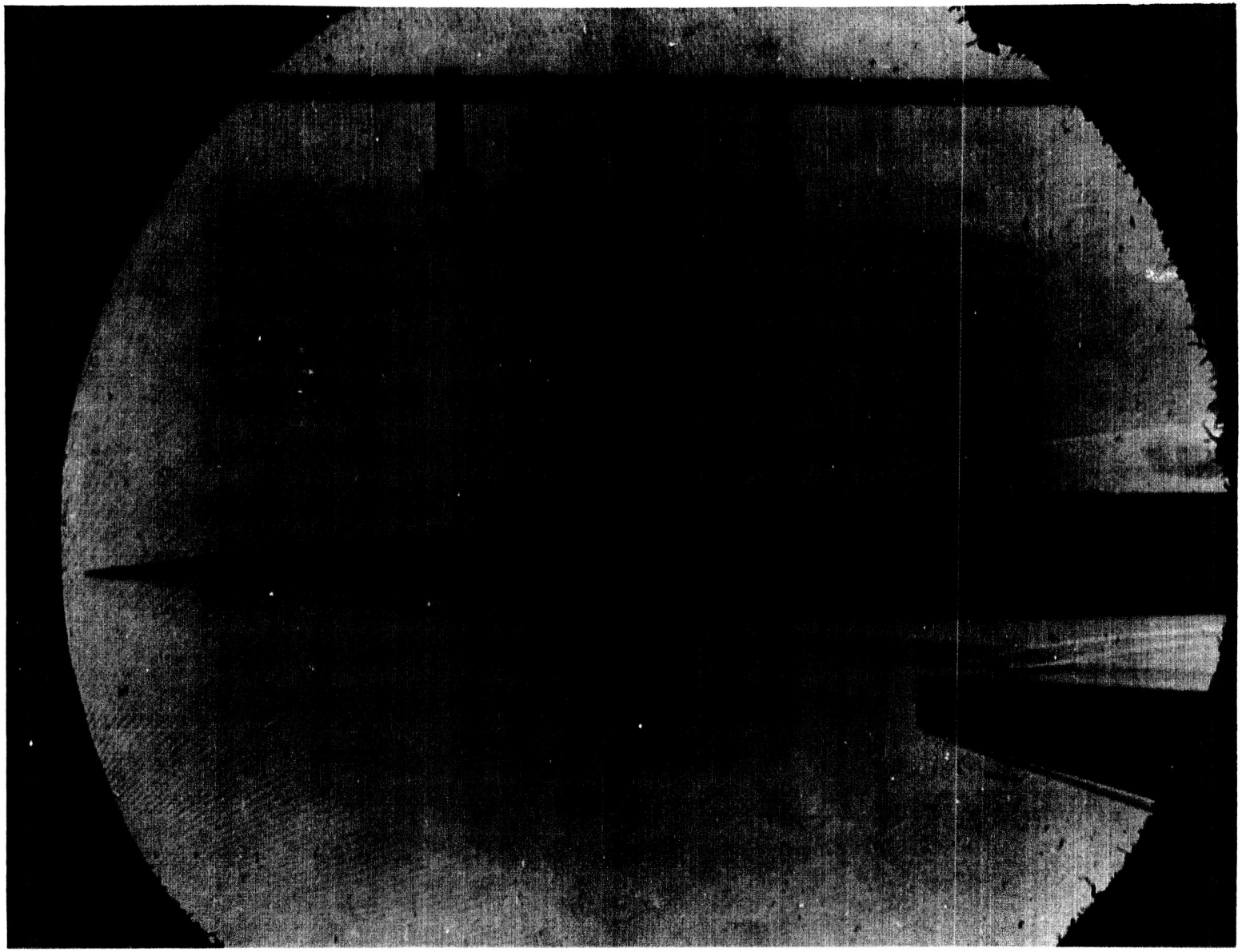

FIGURE 24 FLOW ABOUT SHARP NOSED GRAPHITE MODEL AT MACH NO. = 17.3 AND REYNOLDS NO. = 1.12 X 10^6/FT. (BEFORE CONDITIONING)

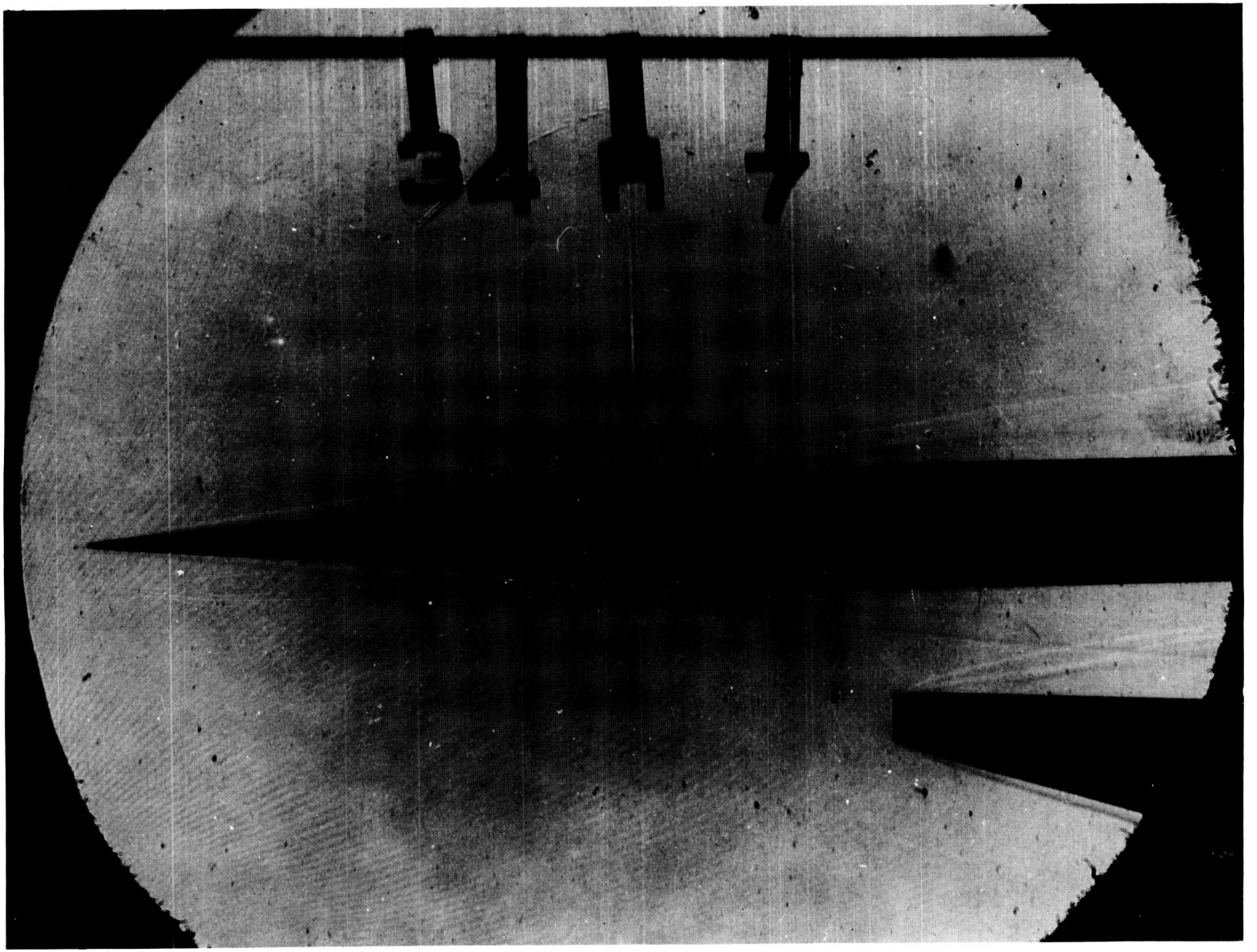

FIGURE 25 FLOW ABOUT SHARP NOSED GRAPHITE MODEL AT MACH NO. = 17.5 AND REYNOLDS NO. = 1.018 X 10^6/FT. (AFTER CONDITIONING)

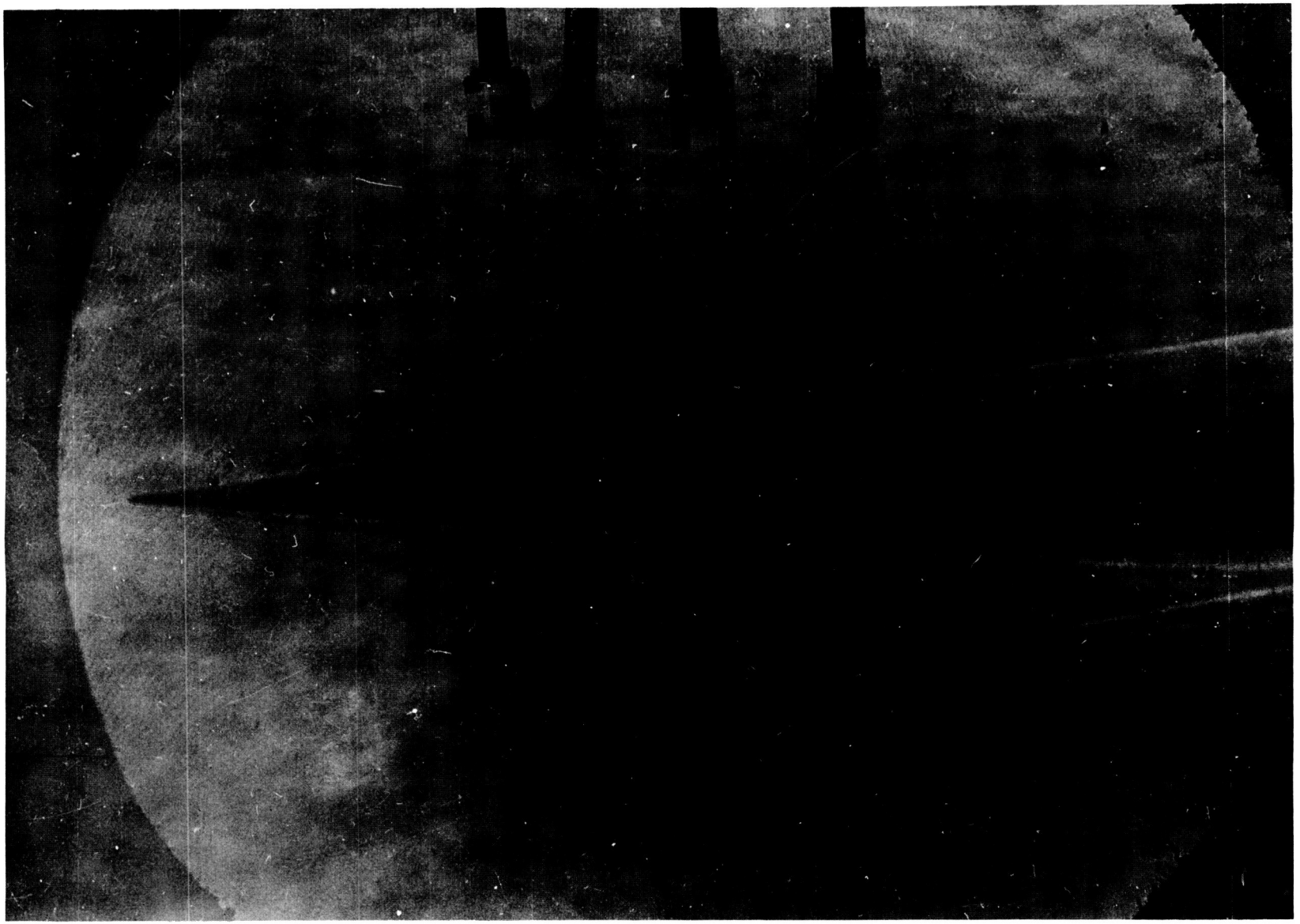

FIGURE 27 FLOW ABOUT SHARP NOSED GRAPHITE MODEL AT MACH NO. = 14.6 AND REYNOLDS NO. = 3.9 X 10^6/FT. (AFTER CONDITIONING)

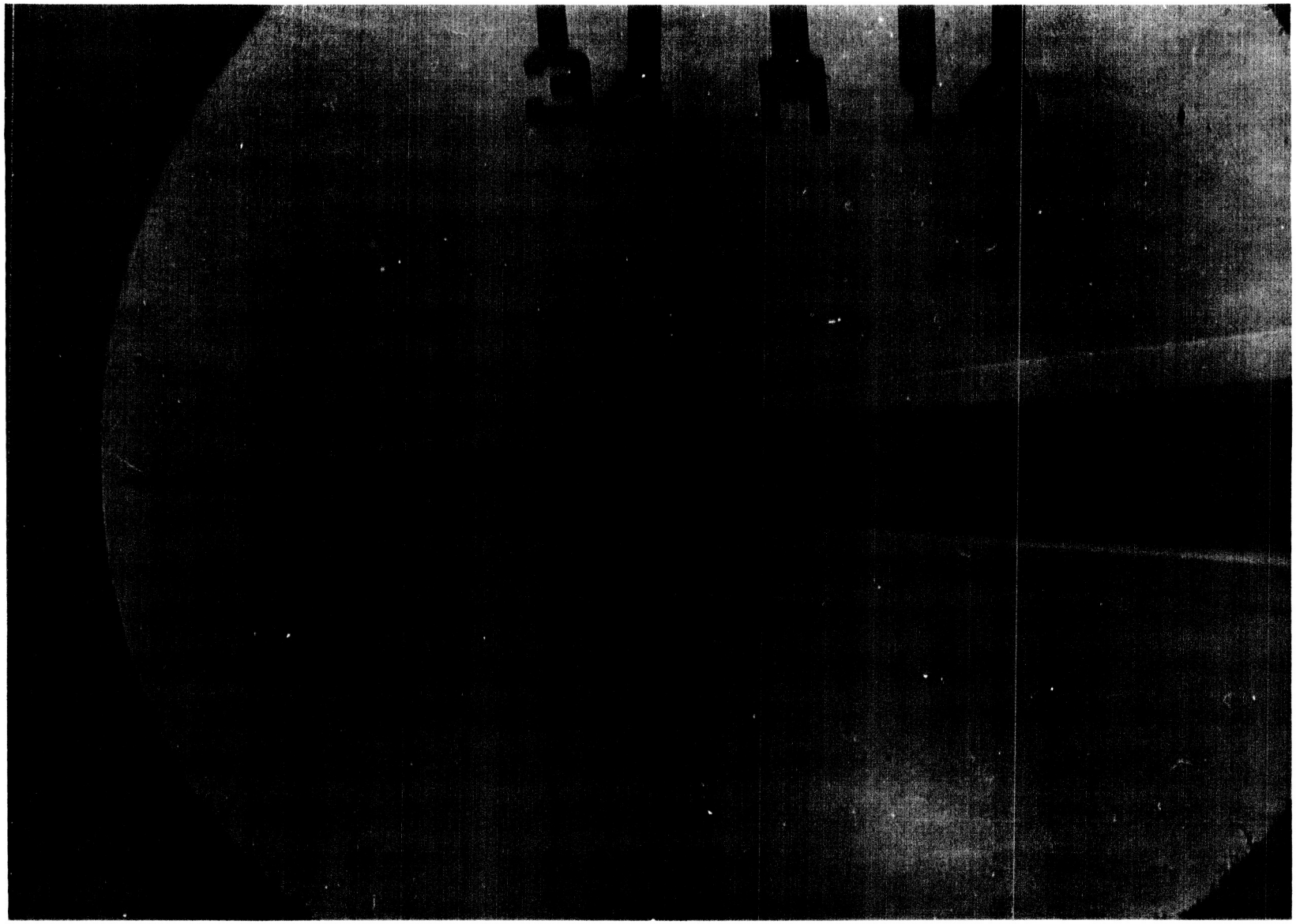

FIGURE 28 HVWT MODEL AT MACH NO. = 14.5 AND REYNOLDS NO. = 3.2 X 10^6/FT. R = 0.00"

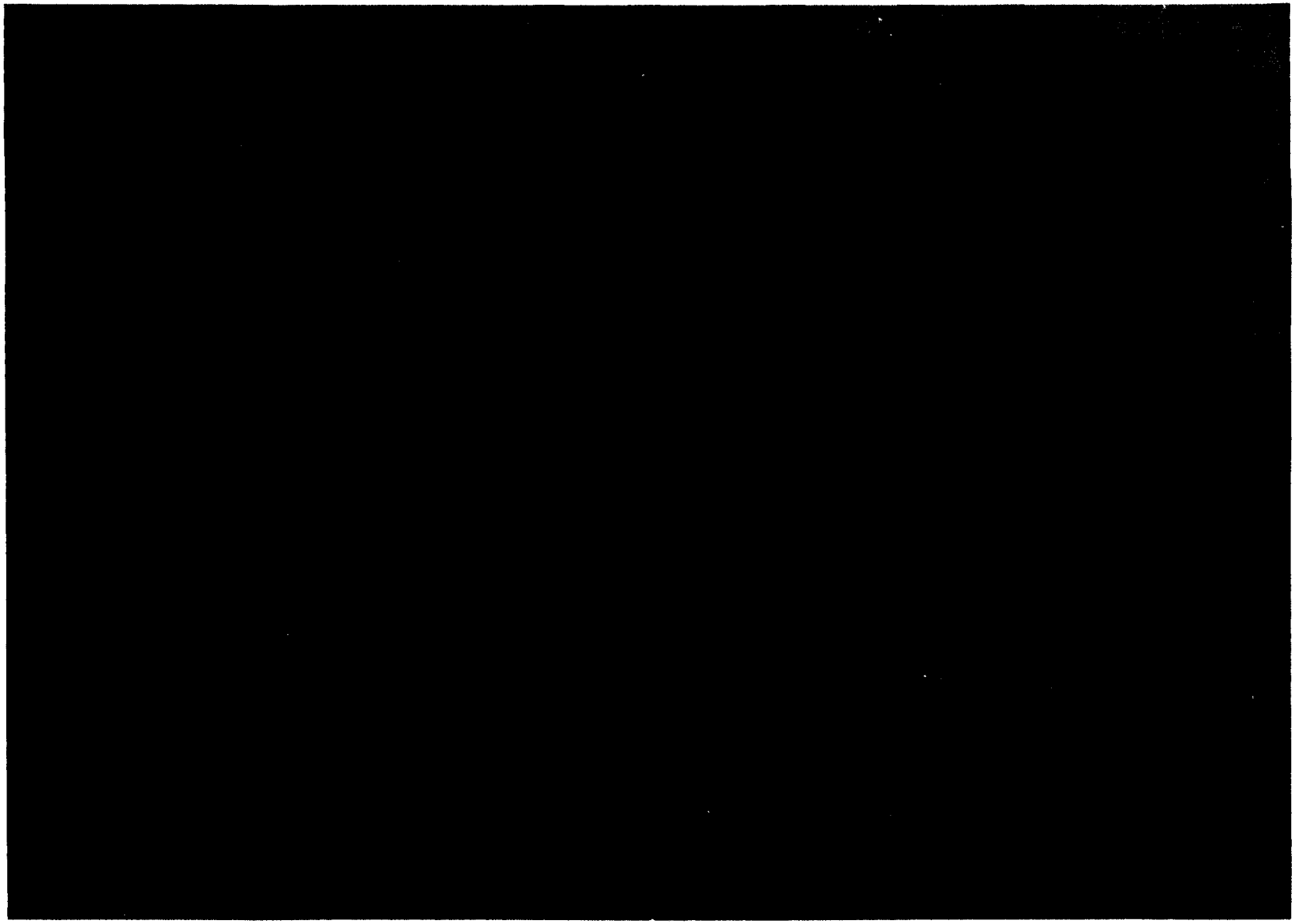

FIGURE 28 HVWT MODEL AT MACH NO. = 14.5 AND REYNOLDS NO. = 3.2 X 10^6/FT. R = 0.00"

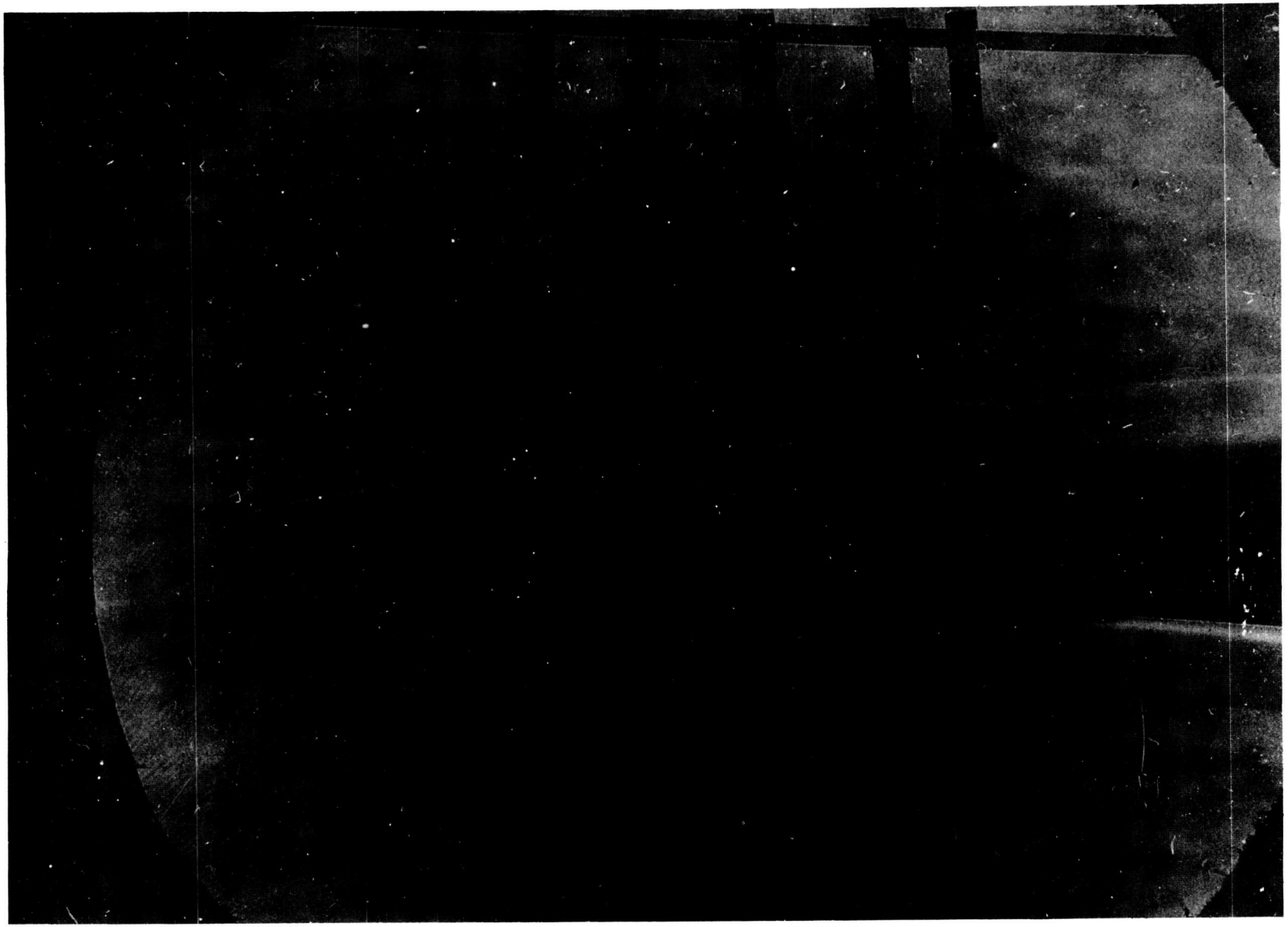

FIGURE 29 HVWT MODEL AT MACH NO. = 14.5 AND REYNOLDS NO. = 3.2 X 10^6/FT. R = 0.05''

4.0 DISCUSSION OF RESULTS

4.1 SHARP CONE

Based on the heat transfer data obtained in the Hypervelocity Wind Tunnel and the pointed configuration which was maintained on the plasma model, it appears that the heating rates near the nose of the sharp cone are less than those predicted by continuum theory.

If one applies the normal criterion for the existence of continuum flow, which is

$$M/\sqrt{R_{e_x}} \leq 0.01 \qquad (7)$$

to the conditions of the HVWT tests, the Reynolds number required for continuum flow is obtained, i.e.

$$R_{e_{x\,(\text{CONTINUUM})}} \geq (14^2)(10^4) = 1.96 \times 10^6 .$$

The heating data for the HVWT test conditions appear to indicate that continuum flow for these high Mach numbers does not exist on the tip of the cone forward of the point where the local Reynolds number is approximately 10^5. This Reynolds number is compatible with the 10^6 value obtained by theory when the uncertainties associated with the 0.01 value of (7) are taken into account.

If the sharp cone does not experience continuum heating over the front portion of the tip, then one might expect a heating distribution over the cone which is typified by the following sketch,

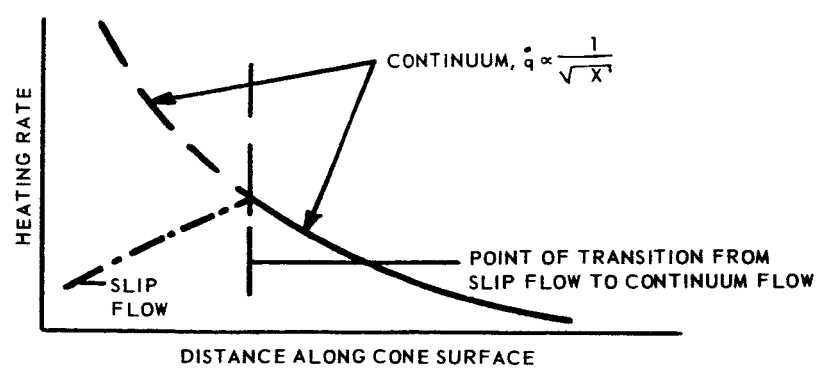

where the heating near the tip of the cone is in the slip flow regime. Since the heating levels associated with slip flow are lower than continuum values, the observed data appears reasonable.

According to diffusion controlled oxidation theory, the recession rate is directly proportional to the heating rate. Consequently, the maximum mass loss rate would occur at the point of maximum heating (which coincides with the point of transition from slip to continuum flow shown in the figure) and would decrease as one approaches the nose.

Based on this slip flow analysis, it seems reasonable to assume that a sharp tip will remain sharp as long as the distance from the tip to the point where maximum heating occurs is greater than the nose radius. Under the conditions where this theory applies, the shock wave would be attached, and the tip material must be one which sublimes rather than melts.

The tendency to maintain a pointed configuration is further strengthened by a pure continuum heating analysis if the heating area is considered. Continuum theory predicts

$$\dot{q}_{NOSE} \propto \frac{1}{(R)^{1/2}}$$

but

$$\dot{q}_{NOSE} \cdot A_{NOSE} \propto \frac{1}{(R)^{1/2}} \cdot R^2 = R^{3/2}.$$

Consequently, for a sharp-tipped cone, the heat input to the extreme tip should approach zero when the available area is considered.

In order to apply the slip flow results to the re-entry flight case for a sharp cone, one divides the Reynolds number for transition from slip to continuum flow by the local Reynolds number per unit length at the particular time of interest. This ratio produces the distance aft of the sharp point where transition flow begins. If this distance is greater than the nose radius, and the shock is attached, the graphite tip experiences a heating distribution similar to that given previously and the tip is assumed to remain sharp. Once the distance to transition approaches the nose radius, blunting is assumed to begin.

Calculations of this type have been performed for conditions corresponding to a flight velocity of 20,000 ft/sec at altitudes of 80,000 feet, 60,000 feet, and 40,000 feet for values of the free stream Reynolds number at transition of 10^4, 10^5, and 10^6, where this spread in Reynolds number was used due to the uncertainties that exist in evaluating the transition point. The results of these calculations are shown in Table V. Some deviation between continuum theory and experimental data was observed at a Reynolds number of 10^5. If the Reynolds number corresponding to the transition point is somewhat less, about 10^4, then the calculations indicate a nose radius of 0.001 inches (which is approximately the grain size of the graphite and appears to be the smallest radius attainable) should be maintained down to an altitude of approximately 40,000 feet, at which time blunting would begin.

TABLE V

EXTENT OF SLIP FLOW ON SHARP CONE
FLIGHT VELOCITY = 20,000 FT/SEC

Altitude (Kilofeet)	Free Stream Reynolds No. Per Foot	Length of Slip Flow Region (Inches) Reynolds Number Required for Transition		
		10^4	10^5	10^6
80	5.8×10^6	0.0207	0.207	2.07
60	1.41×10^7	0.0085	0.085	0.85
40	3.84×10^7	0.00312	0.0312	0.312

4.2 SPHERICALLY BLUNTED CONE

It was noted in Section 3.2 that good agreement was obtained between the measured heat transfer data obtained in the plasma jet tests reported herein and the heating data inferred from erosion measurements made in reference 1. Consequently, the techniques used in reference 1 for predicting the blunting of initially spherical tips during re-entry appear to be substantiated, and the re-entry predictions shown in reference 1 for the blunted tips are unchanged as a result of this study.

5.0 CONCLUSIONS

The conclusions which were reached as a result of the tests described in this report are:

(a) The theories of Fay and Riddell, Lees and Van Driest are considered adequate to predict the heating rates to spherically blunted conical bodies for high Mach number atmospheric re-entry if viscous interaction corrections are applied to the side heating rates computed by these methods.

(b) The stagnation values predicted by Fay and Riddell cease to be valid when the nose radius becomes small compared to the mean free path.

(c) The shoulder to stagnation point mass loss ratios reported by Medford and Holt (Reference 1) were in reasonable agreement with the heating rate ratios obtained in these tests.

(d) Slip flow effects near the tip must be considered when the nose tip has a radius which is less than approximately 0.01 inches.

(e) Based on the slip flow analysis, it is postulated that a graphite tip with a nose radius of 0.001 inches will remain sharp down to an altitude of approximately 40,000 feet at which time blunting will begin.

(f) Conclusion(e)is based on zero angle of attack considerations. A sharp, spinning cone body at angle of attack would probably remain sharp provided the tip material has sufficient strength to withstand the aerodynamic loading.

5.1 RECOMMENDATIONS

It is recommended that further studies be conducted which will produce more information on slip flow effects. This could be achieved in the HVWT by the use of a segmented conical model made from alternate sections of copper and boron nitride, an insulator. The pointed nose calorimeter would be made as small as possible, and the copper segments as thin as possible to obtain true local heating values. The copper segments would be instrumented with thermocouples and the heating values obtained for various Reynolds numbers. The data would then be compared to continuum theory, and a better evaluation of the point where continuum flow begins would be obtained. Based on these findings, one could better predict the performance of pointed cones during re-entry.

LTV Astronautics Division,
LTV Aerospace Corporation,
Dallas, Texas, December 17, 1965.

REFERENCES

1. J. Medford and R. B. Holt, "Study of Graphite Nose Tips for High Reynold's Number Experiments," LTV Astronautics Division Report No. 00.628, May 1965.

2. D. J. Tillian, "Plasma Arc Facilities in the United States," LTV Research Center Report No. 0-71000/3R-22, November 1963.

3. J. L. Lindsey, "Hypervelocity Wind Tunnel Handbook," LTV Aeronautics Division Report No. 2-59740/4R-2150.

4. J. A. Fay and F. R. Riddell, "Theory of Stagnation Point Heat Transfer in Dissociated Air," Journal of the Aeronautical Sciences, pp. 73-121, February 1958.

5. Lester Lees, "Laminar Heat Transfer over Blunt-Nosed Bodies at Hypersonic Flight Speeds," Jet Propulsion, pp. 259-274, April 1956.

6. E. R. Van Driest, "Investigation of Laminar Boundary Layer in Compressible Fluids Using the Crocco Method," NASA TN 2597, January 1952.

7. R. F. Probstein, "Interacting Hypersonic Laminar Boundary Layer Flow Over a Cone," Tech. Report AF 2798/1, Brown University, March 1955.

8. E. R. G. Eckert and R. M. Drake, Jr., Heat and Mass Transfer, pp. 276-285, McGraw-Hill, 1959.